MOLECULAR BIOLOGY

HSF2 cooperates with HSF1 to drive a transcriptional program critical for the malignant state

Roger S. Smith[1,2,3,4]†, Seesha R. Takagishi[1,2,3,5,6]†‡, David R. Amici[1,2,3,4], Kyle Metz[1,2,3], Sitaram Gayatri[1,2,3], Milad J. Alasady[1,2,3], Yaqi Wu[1,2,3,7], Sonia Brockway[1,2,3], Stephanie L. Taiberg[1,2,3], Natalia Khalatyan[2,8], Mikko Taipale[9,10,11], Sandro Santagata[12,13,14], Luke Whitesell[10], Susan Lindquist[15,16,17]§, Jeffrey N. Savas[2,8], Marc L. Mendillo[1,2,3]*

Heat shock factor 1 (HSF1) is well known for its role in the heat shock response (HSR), where it drives a transcriptional program comprising heat shock protein (HSP) genes, and in tumorigenesis, where it drives a program comprising HSPs and many noncanonical target genes that support malignancy. Here, we find that HSF2, an HSF1 paralog with no substantial role in the HSR, physically and functionally interacts with HSF1 across diverse types of cancer. HSF1 and HSF2 have notably similar chromatin occupancy and regulate a common set of genes that include both HSPs and noncanonical transcriptional targets with roles critical in supporting malignancy. Loss of either HSF1 or HSF2 results in a dysregulated response to nutrient stresses in vitro and reduced tumor progression in cancer cell line xenografts. Together, these findings establish HSF2 as a critical cofactor of HSF1 in driving a cancer cell transcriptional program to support the anabolic malignant state.

INTRODUCTION

Heat shock factor 1 (HSF1) is the master regulator of the heat shock response (HSR) (*1*), a highly conserved cytoprotective mechanism that induces expression of molecular chaperones, also known as heat shock proteins (HSPs), in response to elevated temperature (*2*). This function of HSF1 has allowed it to serve as a model for inducible gene expression (*3*, *4*) and become the most well-studied member of the HSF family of transcription factors. Evidence accumulating over the past decade has revealed that the gene expression program driven by HSF1 can vary markedly depending on the context in which it is activated. We and others previously defined distinct HSF1 transcriptional programs in cancer cells (*5*, *6*), in fibroblasts of the tumor microenvironment (*7*), in organismal development (*8*), and in response to virus infection (*9*). In some of these physiological contexts (e.g., viral infection), HSF1 drives a compact transcriptional program comprising mostly HSP genes in a manner similar to its function in heat shock. However, in other contexts, especially those characterized by rapid cell growth (e.g., cancer and development), HSF1 promotes gene expression not only of canonical HSP target genes but also of many noncanonical target genes with roles in diverse biological processes. In breast, lung, colon, and other types of cancer, the expression of HSF1 and its transcriptional program is associated with metastasis and patient death (*5*, *10*). While much research has elaborated mechanisms of HSF1 function in response to elevated temperature (*1*, *2*, *4*, *11*), the mechanisms by which HSF1 regulates this distinct transcriptional program to support carcinogenesis remain poorly understood.

Our studies undertaken to increase our understanding of HSF1's role in cancer revealed a prominent interaction with its paralog HSF2. Unlike HSF1, HSF2 plays a limited role in promoting the HSR despite an ability to bind consensus heat shock elements (HSEs) in vitro and in vivo (*4*, *12*–*15*). HSF2 has been described to function in development (*16*), particularly in the contexts of hemin-induced erythroid cell differentiation (*12*) and spermatogenesis (*17*, *18*). HSF2 also modulates responses to select proteotoxic stresses including proteasome inhibition (*19*, *20*), ethanol, and febrile-range thermal stress (*21*, *22*). Studies of HSF2 function in cancer are limited to only a few recent reports and suggest that HSF2 can both promote and suppress cancer cell growth in different cancer models (*23*–*25*). These studies of HSF2, along with studies of HSF1 in cancer, have focused on one or the other HSF without regard to any interplay, but understanding the potential cooperative or antagonistic interactions of these transcription factors is crucial (*26*). Whether these disparate effects of HSF2 are due to a role directly regulating transcription or through a functional link to HSF1's well-established protumorigenic functions is unclear (*27*). Therefore, rigorous characterization of HSF2's role in cancer and its mechanistic interplay with HSF1 are required to shed light on how HSFs support cancer.

In this study, we demonstrate that HSF2 physically interacts with HSF1 in cancer cells, resulting in an indistinguishable pattern of genome occupancy. Across breast, prostate, colon, and lung cancers, HSF2 regulates expression of HSF-bound genes, including

[1]Department of Biochemistry and Molecular Genetics, Northwestern University Feinberg School of Medicine, Chicago, IL 60611, USA. [2]Simpson Querrey Institute for Epigenetics, Northwestern University Feinberg School of Medicine, Chicago, IL 60611, USA. [3]Robert H. Lurie Comprehensive Cancer Center, Northwestern University Feinberg School of Medicine, Chicago, IL 60611, USA. [4]Medical Scientist Training Program, Northwestern University Feinberg School of Medicine, Chicago, IL 60611, USA. [5]Department of Biochemistry and Biophysics, UCSF, San Francisco, CA 94158, USA. [6]Tetrad Graduate Program, UCSF, San Francisco, CA 94143, USA. [7]Master of Biotechnology Program, Northwestern University, Evanston, IL 60208, USA. [8]Department of Neurology, Northwestern University Feinberg School of Medicine, Chicago, IL 60611, USA. [9]Donnelly Centre for Cellular and Biomolecular Research, University of Toronto, Toronto, ON, Canada. [10]Department of Molecular Genetics, University of Toronto, Toronto, ON, Canada. [11]Molecular Architecture of Life Program, Canadian Institute for Advanced Research (CIFAR), Toronto, ON, Canada. [12]Department of Pathology, Brigham and Women's Hospital and Harvard Medical School, Boston, MA 02115, USA. [13]Laboratory of Systems Pharmacology, Harvard Medical School, Boston, MA 02115, USA. [14]Ludwig Center at Harvard, Boston, MA 02115, USA. [15]Whitehead Institute for Biomedical Research, Cambridge, MA 02142, USA. [16]Massachusetts Institute of Technology, Cambridge, MA 02142, USA. [17]Howard Hughes Medical Institute, Cambridge, MA 02139, USA.
*Corresponding author. Email: mendillo@northwestern.edu
†These authors contributed equally to this work.
‡Present address: Department of Biochemistry and Biophysics, University of California–San Francisco, San Francisco, CA 94158, USA.
§Deceased.

both canonical HSPs and noncanonical factors involved in cell metabolism and proliferation. Regulation of these genes by HSF2 is critical for the cellular response to cancer-associated stressors in a manner distinct from its dispensable role in the HSR. Lastly, HSF2 is required for cell line xenograft progression, and as a result, HSF2 loss extends tumor-bearing mouse survival. These findings identify HSF2 as a critical accomplice of HSF1 in driving protumorigenic gene expression programs and indicate that the role of HSF2 in cancer biology is far greater than previously appreciated.

RESULTS

HSF2 interacts with HSF1 in diverse cancers

To identify protein interacting partners of HSF1 in cancer, we stably expressed HSF1 tagged with a 3xFLAG-V5 epitope in a panel of four cancer cell lines and used anti-FLAG beads to perform immunoprecipitation (IP) followed by liquid chromatography tandem mass spectrometry (LC-MS/MS)–based proteomic analysis. HSF2, the highest expressed HSF1 paralog in human tumors (fig. S1A), emerged as a high-confidence interacting protein in each of the four cell lines tested (Fig. 1A). We subsequently performed the reciprocal experiment and recovered HSF1 from HSF2-FLAG in two of the three lines tested. Although we were unable to detect HSF1 in HSF2 IP of ZR-75-1 cell lysates, we identified lower amounts of HSF2 itself, perhaps due to a mechanism limiting HSF2 expression or IP efficiency in that cell line. Additional interacting proteins include those involved in cellular metabolism and cytoskeletal organization, but none of these interacting proteins are observed as consistently as HSF2 in the cancer cell lines tested (fig. S1B).

As an orthogonal strategy to identify HSF1-interacting proteins, we adopted LUMIER, a quantitative, high-throughput protein-protein interaction assay previously used to study chaperone-client interactions (*28*, *29*). Briefly, we transiently expressed a collection of FLAG-tagged plasmids ("the bait") in a 293T cell line that stably expressed HSF1 tagged with Renilla luciferase ("the prey"). The bait collection consisted of 2853 unique clones comprising most transcription factors along with many other genes involved in chromatin regulation, protein synthesis, and posttranslational modification (table S2). After lysis, the bait proteins were individually captured with anti-FLAG–coated 384-well plates, and luminescence (i.e., HSF1 concentration) was measured. Of the 2853 clones, HSF2 was the top HSF1-interacting transcription factor (Fig. 1B, fig. S1C, and table S2). Overall, only the HSF1 control (due to homo-oligomerization) and two HSP70 family proteins, known to strongly interact with HSF1 (*30*, *31*), scored higher. We further validated these findings using co-IP of endogenous HSF1 and immunoblot analysis of endogenous HSF2 in a panel of cancer cell lines including breast, prostate, and lung cancer (Fig. 1C). Thus, HSF1 and HSF2 physically interact in cancer cells.

To explore the functional significance of this protein interaction in cancer cells, we performed an electrophoretic mobility shift assay (EMSA) to test whether HSF2 and HSF1 can each bind the canonical HSE found within the promoter of *HSPA8*, a site bound by HSF1 with high affinity in cancer cells (Fig. 1D). A DNA duplex harboring the *HSPA8* HSE was incubated with cancer cell lysates in the presence or absence of a control immunoglobulin G (IgG), HSF1, or HSF2 antibodies. Proteins in cell lysates interacted with the *HSPA8* promoter, causing a specific electrophoretic band shift that could be competed away with a 20× excess of unlabeled *HSPA8* HSE, but not with a mutant *HSPA8* HSE containing three substitutions in nucleotides critical for HSF1 binding or with the HSE of *HSPA6* (an HSF1 target gene in the HSR that is minimally bound by HSF1 in cancers, but well bound in heat shock) (*5*). Moreover, incubation with HSF1- or HSF2-specific antibodies but not IgG resulted in a supershift, suggesting that the interacting proteins HSF1 and HSF2 can both bind to this same target DNA. The HSF1-HSF2-HSE complex formed using lysates from cancer cells grown under basal conditions was far more robust than that observed for nontumorigenic mouse embryonic fibroblasts (MEFs), which required treatment with proteasome inhibitor, MG132, to stimulate HSF-HSE binding (fig. S1D). These results suggest that HSF2 forms an active complex with HSF1 capable of binding DNA in proliferating cancer cells.

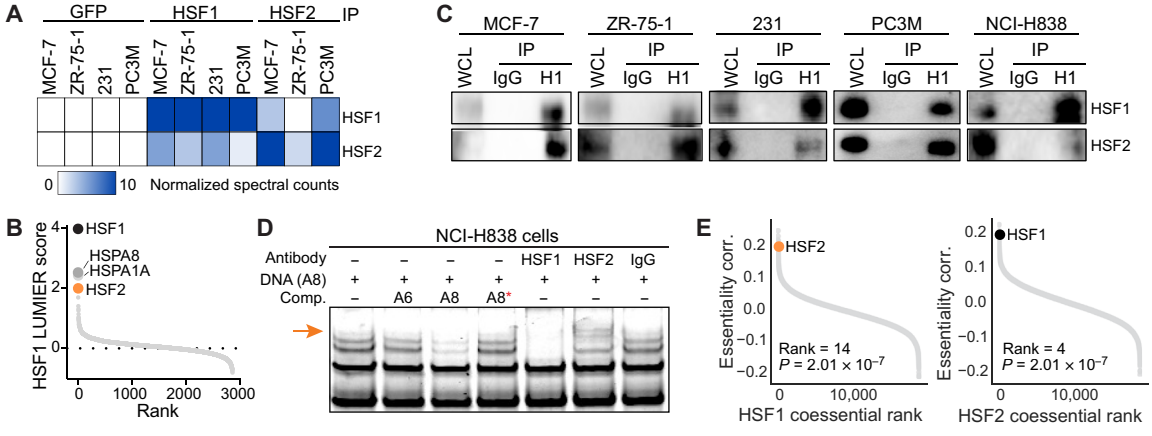

Fig. 1. HSF2 interacts with HSF1 in diverse cancers. (**A**) IP-MS of green fluorescent protein (GFP), HSF1, or HSF2 in four cancer cell lines, indicated. Data for HSF1 and HSF2 are plotted as the number of spectral counts normalized to GFP control. (**B**) HSF1 LUMIER assay reveals HSF2 as the top HSF1-interacting transcription factor. Plot shows ranked HSF1 LUMIER score (GFP-normalized, $\log_2$-transformed luminescence values). (**C**) IP for HSF1 (H1) followed by immunoblot for HSF1 and HSF2. WCL, whole-cell lysates as input; 231, MDA-MB-231. (**D**) EMSA assay using HSPA8 (A8) as bait. Reactions were incubated with HSF1, HSF2, or control IgG antibody as indicated. A6 and A8 represent promoter sequences used for HSPA6 or HSPA8, respectively. A8* indicates a mutated HSE in the competing HSPA8 DNA promoter sequence. An arrow is included to highlight the level of supershift in HSF2 antibody lane. (**E**) Coessentiality rank (*x* axis) and correlation coefficient (*y* axis) for all genes with HSF1 (left) or HSF2 (right). The position of HSF2 or HSF1 in the coessentiality plot is indicated (orange or black dot, respectively).

Physically interacting proteins with cooperative roles in the same process are often critical for optimal cell growth in the same cellular contexts and thus frequently display shared knockout fitness profiles in large-scale genetic screening studies (*32*–*34*). To investigate the extent to which HSF1 and HSF2 have similar fitness requirements in cancer cells, we applied a bias-adjusted, rank-based coessentiality approach to whole-genome dependency data from over 700 diverse cancer cell lines (*35*–*37*). Our analysis revealed that HSF1 and HSF2 have strongly correlated patterns of cancer cell essentiality (r = 0.184, P = 2.01 × 10^{-7}; Fig. 1E). *HSF2* is the 14th ranked coessential gene with *HSF1* and the highest ranked transcription factor (Fig. 1E, left). Similarly, *HSF1* is *HSF2's* fourth rank most similarly essential gene (Fig. 1E, right). Together, the physical interaction, cancer cell HSE-binding activity, and correlated cancer cell essentiality profiles of HSF1 and HSF2 suggest that these factors have a critical shared function in cancer.

HSF2 shares chromatin occupancy sites with HSF1 in cancer cells

For a more global view of HSF2 function in cancer, we assayed its chromatin occupancy using chromatin IP followed by sequencing (ChIP-seq) in two aggressive cancer cell lines: a triple negative breast cancer cell line (MDA-MB-231) and a metastatic prostate cancer cell line (PC3M). We first validated our HSF2 antibody by performing immunoblot analysis using purified recombinant polyhistidine-tagged maltose binding protein (HIS-MBP)–HSF1 and HIS-MBP–HSF2 to demonstrate antibody specificity and lack of paralog cross-reactivity (fig. S1, E to H). Using a previously validated HSF1 antibody (*5*) and the validated HSF2 antibody for ChIP-seq in MDA-MB-231 cells, we identified 677 regions bound by HSF2 or HSF1, with a strong pattern of co-occupancy (Fig. 2A and fig. S2C). Motif analysis demonstrated a strong enrichment for the consensus HSE (P = 1 × 10^{-217}) (Fig. 2B). Among bound regions observed in MDA-MB-231, most occurred at intergenic or intronic loci (fig. S2B). PC3M cells yielded similar results with 794 regions bound by either HSF2 or HSF1, many of which were co-occupied (Fig. 2F). In addition, at regions called peaks only for HSF1, HSF2 was present at lower levels as demonstrated in all heatmaps that plot the union of HSF1 and HSF2 peaks and depict indistinguishable occupancy patterns (Fig. 2F and fig. S2, G and I). Motif analysis of these regions similarly revealed the HSE as the most significantly enriched motif (P = 1 × 10^{-31}; Fig. 2G). Most binding occurred at promoter sites in PC3M, similar to other cell lines with high levels of HSF1 activation (fig. S2H) (*5*). Co-occupied genes in both cell lines included HSP targets (e.g., *HSP90AB1*, *HSPA8*, and *HSPA1B*) and non-HSPs (e.g., *RBM23* and *CKS2*; Fig. 2, C and H).

To determine the ability of either HSF2 or HSF1 to bind chromatin in the absence of its paralog, we performed ChIP-seq for each factor in cells with the other factor knocked out (e.g., HSF2 ChIP in HSF1 knockout cells) (immunoblots in fig. S2, F and J). In MDA-MB-231 cells, loss of HSF1 resulted in a global reduction in HSF2 chromatin occupancy (Fig. 2D and fig. S2D). This result is consistent with previous data demonstrating that HSF2 requires HSF1 for maximal *HSP70* promoter binding (*38*). In HSF2 knockout cells, there was an increase in HSF1 bound to chromatin compared with controls, perhaps reflecting a replacement of HSF2 in active heteromeric complexes (Fig. 2E and fig. S2E). We did not observe changes in the genomic loci where this HSF1 homo-oligomer binds when HSF2 is depleted. In PC3M cells, loss of HSF1 also resulted in reduced HSF2 chromatin occupancy (Fig. 2I). In this cell line, however, some loss of HSF2 chromatin occupancy is attributable to reduced total HSF2 protein levels (fig. S2J). HSF1 chromatin occupancy in HSF2-depleted cells was not noticeably changed (Fig. 2J). Together, these results suggest that while HSF2 is dispensable for HSF1 chromatin occupancy, HSF1 can promote HSF2 chromatin occupancy through either its effects on HSF2 protein stability or on HSF2 DNA binding (figs. S2D and S3A) (*16*, *20*, *38*, *39*). More broadly, the nearly identical HSF2 and HSF1 chromatin occupancy landscape in two distinct types of cancer cell lines with different levels of HSF1 and HSF2 activity, along with their highly correlated effects on cell growth across hundreds of human cancer cell lines, supports the likelihood that these factors regulate transcription of similar genes in cancer cells.

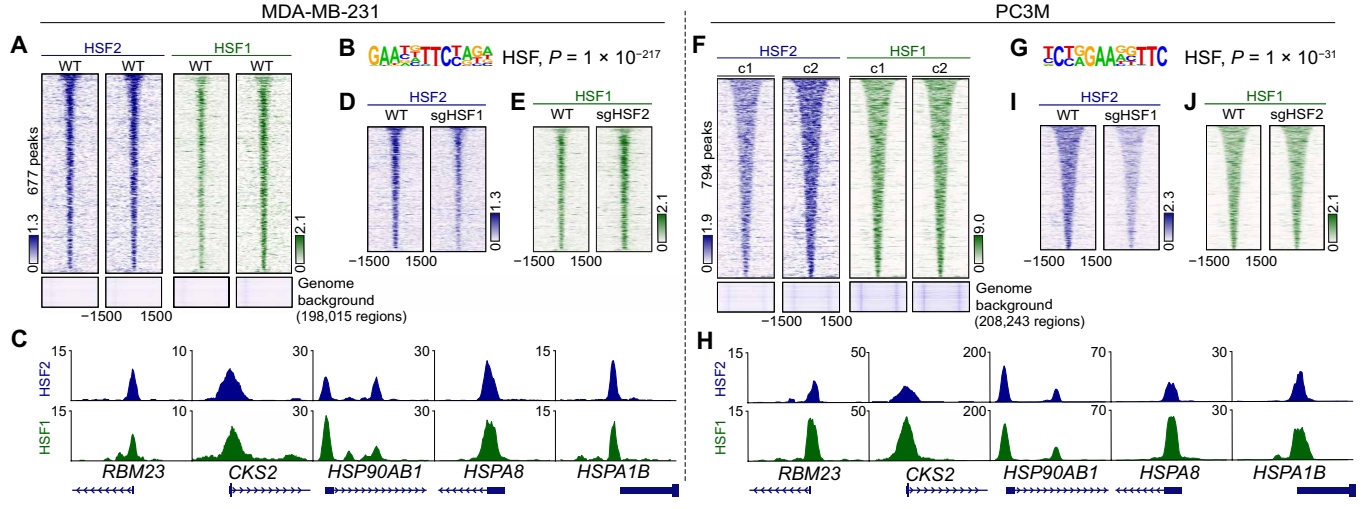

Fig. 2. HSF2 shares chromatin occupancy sites with HSF1 in cancer cells. (**A** and **F**) ChIP-seq for HSF2 or HSF1 in the indicated cell line. Dual tracks indicate biological replicates. (**B** and **G**) Enriched motifs of ChIP peaks. (**C** and **H**) Example ChIP-seq tracks for HSF2 and HSF1 at five loci implicated in HSF cancer programs. (**D**, **E**, **I**, and **J**) ChIP-seq tracks for HSF1 or HSF2 in HSF knockout cells as indicated. These data merged all replicates for ease of visualization. WT, wild-type, parental cell lines. c1 and c2 represent cell lines expanded from a single wild-type cell clone as control for clonal CRISPR knockouts.

HSF2 drives a protumorigenic transcriptional program

To investigate how HSF2 affects cancer cell gene expression and how this relates to HSF1 activity, we performed RNA sequencing (RNA-seq) to measure gene expression in a panel comprising 11 cancer cell lines treated with short-interfering RNA (siRNA) pools targeting HSF1, HSF2, or non-targeting (NT) controls. The cancer cell lines profiled cover the most common and lethal cancers: luminal and basal breast cancers (*40*), along with prostate, lung, and colon cancers. We focused our assessment of gene expression changes on those most significant [false discovery rate (FDR)–adjusted $P < 0.05$] and conserved across these diverse cell line backgrounds (see Materials and Methods). Using these stringent parameters, knockdown of HSF2 resulted in 32 or 10 genes with either reduced or elevated levels, respectively. HSF1 knockdown resulted in 167 or 164 genes with either reduced or elevated levels, respectively.

K-means clustering of the union of differentially expressed genes upon acute depletion of either HSF revealed five major clusters (Fig. 3A). Clusters 1 and 2 contained genes whose expression decreased upon HSF2 and HSF1 depletion, indicating that they are positively regulated by both HSFs. Gene set enrichment analysis (GSEA) of this group of genes revealed a strong enrichment for genes annotated as cell cycle [FDR-adjusted $Q = 4.3 \times 10^{-8}$], HSF1 activation ($Q = 1.0 \times 10^{-11}$), RNA binding ($Q = 7.1 \times 10^{-11}$), and protein folding ($Q = 1.3 \times 10^{-07}$). These clusters reveal similar regulation of gene expression by HSF2 and HSF1. Not all genes in these clusters are significantly differentially expressed for HSF2 depletion across all cell lines using an FDR-adjusted *P* value less than 0.05; however, HSF2 depletion still reduces expression of most target genes in these clusters (Fig. 3, A and B). Cluster 3 contained genes generally positively regulated by HSF1 but not HSF2 and enriched for cell cycle processes ($Q = 1.4 \times 10^{-37}$) and protein folding ($Q = 3.8 \times 10^{-7}$). Clusters 4 and 5 contained many genes that had increased expression upon HSF2 or HSF1 depletion. These genes were enriched in processes that include autophagy ($Q = 3.3 \times 10^{-7}$), and protein localization ($Q = 4.9 \times 10^{-5}$). Notably, HSF2 regulates both canonical HSP targets (e.g., *HSP90AB1*, *HSPH1*, and *HSPE1*) and non-HSP (e.g., *CKS1B* and *JARID2*) targets previously attributed to HSF1 in cancer gene expression programs, highlighted in Fig. 3B. Thus, the highly concordant changes in the cancer cell transcriptome resulting from loss of either HSF are consistent with a model of cooperative gene expression regulation.

To identify direct transcriptional targets of HSF2 and HSF1, we integrated our ChIP-seq and RNA-seq data (Fig. 3A, right heatmap). Many regulated genes in clusters 1 to 4 are also bound by HSF2 and HSF1. In clusters 4 and 5, fewer genes are bound, suggesting that most of the increases in gene expression conserved across cancers occur as a downstream consequence of HSF loss. Focusing only on HSF-bound genes highlights an extraordinarily similar program of cancer cell gene regulation by HSF2 and HSF1, with many bound genes exhibiting reduced expression upon depletion of either HSF, despite some variation in the strength of regulation (fig. S3B). Together, the chromatin binding and gene expression data demonstrate that HSF2 activates many of the same targets as HSF1 in cancer. Thus, considering the previously established link between HSF1 activity in cancer cells, its protumorigenic phenotypes in

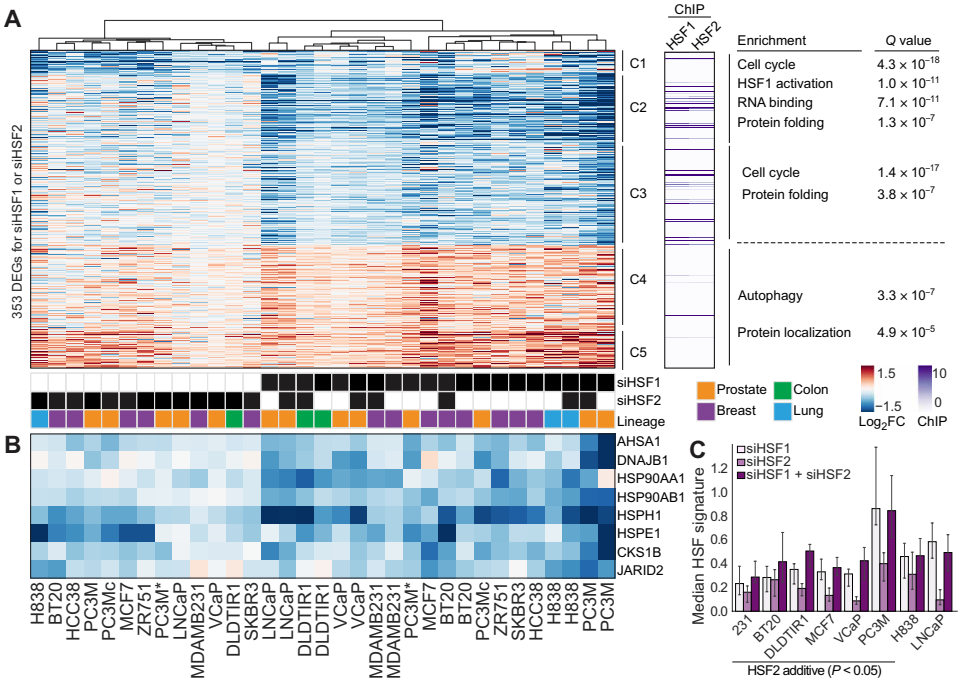

Fig. 3. HSF2 drives a protumorigenic transcriptional program. (**A**) RNA-seq data of 11 cancer cell lines treated with either siRNA targeting HSF1 (siHSF1) or siHSF2 or both. Data are expressed as $\log_2$ fold change ($\log_2$FC) versus the NT control in the respective cell line. The heatmap contains genes called significant for siHSF1, siHSF2, or both by EdgeR. Relative ChIP-seq binding intensity is plotted to the right of the heatmap for both HSF1 and HSF2. GSEA was performed and select enriched gene ontology (GO) terms are displayed along with their FDR-adjusted *P* value (*Q* value). (**B**) Select target genes from (A) are highlighted. PC3Mc, clonally derived, wild-type PC3M; PC3M*, wild-type population with On-Target Plus siRNA as opposed to siGenome siRNA for "PC3M." (**C**) Median absolute $\log_2$ fold change signature strength for ChIP-bound genes in (A) for cell lines receiving single and double siRNA treatment. Data are plotted as median ± 95% confidence interval. Additivity was tested (see Materials and Methods) and indicated where $P < 0.05$; see also fig. S4 (fig. S4, B and D).

animal models, and the expression of HSF1's transcriptional targets as a coherent program in human tumors associated with poor clinical outcomes in patients (*5*, *10*, *41*, *42*), these data suggest that HSF2 likewise promotes this transcriptional program critical for the malignant state.

While HSF2 and HSF1 drive expression of similar genes, the magnitude of changes observed with HSF2 depletion was generally less than that of HSF1 depletion for many genes, which could be influenced by differences in chromatin binding or protein levels. We did not find differences in relative binding of these genes between HSF1 and HSF2 in any cluster that would explain this difference (fig. S3C). To better quantify the effect of each HSF on gene regulation, we used the absolute value of $\log_2$-normalized fold change data for "HSF cancer signature," defined as ChIP-bound genes that are differentially expressed across cancer cell lines. We next assessed how the expression levels of each HSF paralog in a cell might affect the strength of the HSF cancer signature by quantifying total HSF1 and HSF2 in cell lysates using an immunoblot with purified protein standards (fig. S3, D to F). The total protein level of HSF1 is far greater than that of HSF2 in each cell line. However, the protein expression levels of HSF2 did not significantly correlate with the strength of the siHSF2 gene expression signature ($r = 0.3$, $P = 0.48$; fig. S3G), in contrast to HSF1 protein expression levels correlating with the siHSF1 gene expression signature ($r = 0.86$, $P = 6e{-}3$) (fig. S3H).

Another possible explanation for the stronger effect of HSF1 depletion on transcription in cancer cells is that HSF2 protein levels were also reduced after HSF1 depletion (fig. S3A), making HSF1-depleted cells functionally closer to an HSF1/HSF2 double knockdown. This idea is also supported by our observation that HSF1 depletion reduced global HSF2 chromatin occupancy (Fig. 2, D and I). To address this possibility, we simultaneously depleted HSF1 and HSF2 in seven cell lines of our original panel. In each cell line tested, HSF1/HSF2 double knockdown tightly clusters with that cell line's HSF1 knockdown sample (Fig. 3A). Comparing the strength of the HSF cancer signature for single and double knockdown samples revealed a partially additive effect of depleting HSF2 in combination with HSF1 depletion (double knockdown) in six of the eight cell lines and an epistatic relationship in LNCaP and H838 (Fig. 3C; statistics in fig. S4, B and D). Some genes exemplifying this pattern of additivity included *HSPH1*, *HSP90AA1*, *CKS1B*, and *JARID2* (fig. S4, A and C). These results suggest that HSF1 and HSF2 cooperate for maximal target gene expression.

Considering HSF2 and HSF1 bind and regulate target genes similarly, we asked whether expressing each HSF paralog could serve to rescue gene expression in the reciprocal knockout. We first engineered MCF7 cells, to express a control green fluorescent protein (GFP)–FLAG, HSF1-FLAG, or HSF2-FLAG construct. Next, we treated each cell line with siRNA targeting HSF2, HSF1, or NT control (fig. S5A) and performed RNA-seq. We examined the high-confidence HSF-bound and transcriptionally regulated genes defined as the HSF cancer signature (fig. S3C) and found that HSF1 overexpression failed to rescue all but a few genes (fig. S5B). These genes included *AZIN1*, *DNAJB1*, and *HSPH1*, which HSF1 overexpression modestly induced in HSF2 knockout cells, but they were not induced in the HSF2 rescue of HSF1-depleted cells. These data suggest that neither HSF can fully function without an intact HSF1-HSF2 complex. Together, these experiments reveal the intertwined roles of HSF1 and HSF2 in cancer, where formation of an HSF complex drives concordant, direct regulation of many genes critical to the cancer gene expression programs regulated by HSF1 and HSF2.

Long-term loss of HSF2 and HSF1 results in sustained suppression of proteostasis gene expression conserved across cancers

While investigating the effects of short-term HSF loss provides insight into their role in gene regulation, it was unknown whether compensatory mechanisms could reestablish equilibrium in a cancer cell lacking HSF2 or HSF1 for a longer period. Considering the similarities of these HSF paralogs in regulating cancer cell gene expression and their strong correlation in effects on cancer cell line growth over a longer duration in CRISPR screening datasets (Fig. 1D), we hypothesized that long-term loss of HSF1 and HSF2 would result in concordant effects on gene expression in a manner similar to short-term depletion. To test this hypothesis, we transduced six cancer cell lines with single-guide RNAs (sgRNAs) targeting HSF2 or HSF1 for CRISPR-Cas9–mediated knockout or an NT sgRNA control and performed RNA-seq (Fig. 4A). To preserve heterogeneity within cell lines, we generated population knockouts where possible (population knockouts failed for PC3M, so we engineered and selected two independent control and knockout clones). While acute (3 days) depletion of HSF1 or HSF2 by siRNA resulted in broadly correlated gene expression profiles such that neither siRNA nor cell line dominated hierarchical clustering (Fig. 4B, left), long-term (>14 days) HSF loss by CRISPR resulted in distinct cell type–specific gene expression changes (Fig. 4B, right). That is, the cell line background was the dominant variable between clusters, rather than which HSF was depleted. This suggests that loss of either HSF provokes an adaptive change that is dependent on the cellular context.

Despite the strong lineage-specific adaptation, we were able to identify a core module of genes with persistent reduced expression following HSF knockout across cell lines (Fig. 4C). Knockout of HSF2 resulted in 17 down-regulated and 9 up-regulated genes. HSF1 knockout resulted in 78 down-regulated and 30 up-regulated genes for a total of 186 unique genes (adjusted $P < 0.05$ for either HSF1 or HSF2 knockout; Fig. 4A). *K*-means clustering of genes revealed patterns of down-regulated genes upon knockout enriched in biological processes including protein folding ($Q = 5 \times 10^{-25}$), DNA biosynthesis ($Q = 3.3 \times 10^{-11}$), and stress response ($Q = 7.8 \times 10^{-09}$). Notably, HSFs directly bind many of these genes in ChIP-seq experiments, especially genes down-regulated with HSF loss (Fig. 4C, right heatmap). These genes not only included many canonical HSPs (e.g., *HSP90*s, *HSPH1*, and *AHSA1*) but also included non-HSPs (e.g., *JMJD6* and *PTOV1*; Fig. 4D). Long-term HSF loss did not substantially affect the expression of proliferation-associated genes (e.g., *CKS1B*), as observed with short-term depletion (Fig. 3). To assess the extent to which depletion of both HSF1 and HSF2 affects gene expression in CRISPR-edited cells, MDA-MB-231 double knockout (dKO) cells were engineered, and gene expression was measured (Fig. 4E). Similar to the many cells lines treated with siRNA targeting both HSF1 and HSF2, MDA-MB-231 dKO cells exhibited stronger down-regulation of genes in the HSF cancer signature than depletion of one HSF or the other. These results are consistent with cooperative activity of these factors as observed in short-term siRNA experiments (Fig. 3, fig. S4).

In addition to the effects on proteostasis gene expression, many cell type–specific changes were observed with HSF loss, suggesting that these transcription factors may directly or indirectly regulate cell state more broadly (fig. S6). These data demonstrate that there are many more differentially expressed genes for each cell line, extending beyond the consensus HSF signature defined in Figs. 3

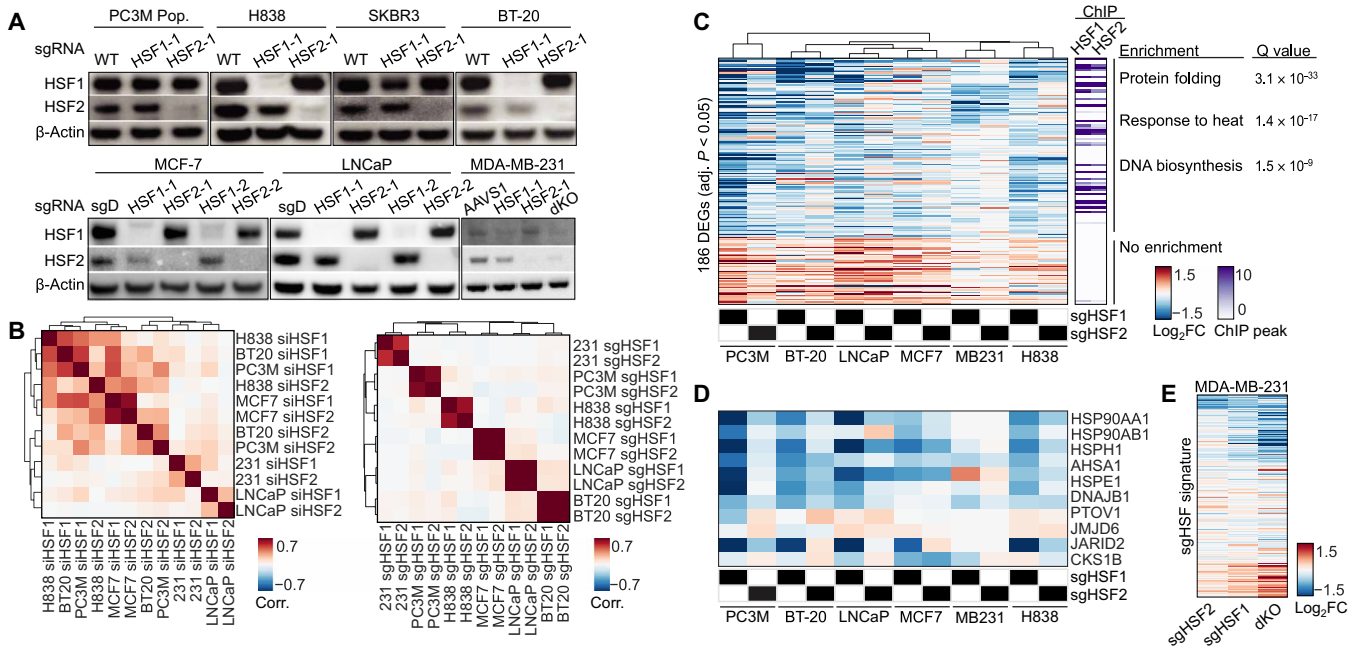

Fig. 4. Long-term loss of HSF2 and HSF1 results in sustained suppression of proteostasis gene expression conserved across cancers. (**A**) Knockout of HSF1 or HSF2 was confirmed by immunoblot. (**B**) Correlation plots of $\log_2$ fold change values for the union of differentially expressed genes for each siRNA-treated sample and each sgRNA knockout sample. (**C**) Differentially expressed genes in either sgHSF1 or sgHSF2 knockout cells for the indicated cell lines. Relative ChIP-seq binding intensity is plotted to the right of the heatmap for both HSF1 and HSF2. GSEA was performed and select enriched GO terms are displayed along with their FDR-adjusted *P* value (*Q* value). (**D**) Select target genes from (A) are highlighted. (**E**) Heatmap of single and double-knockout (dKO) MDA-MB-231 cells, plotting genes from (C).

and 4, highlighting the long-term consequences of HSF loss on tumor cell biology. These results demonstrate that loss of either HSF has durable consequences on gene expression with concordant decreases in proteostasis gene expression programs and further supports the inability of either factor to fully compensate for loss of the other HSF.

HSF2 and HSF1 promote the transcriptional response to cancer-associated stresses

Previous studies using HSF2 knockout MEFs did not identify a significant role for HSF2 in the global response to thermal stress (*4*, *43*). Because we revealed increased activity for HSF2 in cancer cell lines, we wondered whether the HSR in cancer cells might also be more dependent on HSF2. To test this idea, we performed RNA-seq in our HSF2 knockout MDA-MB-231 cell lines grown either at 37°C or following a 42°C heat shock along with wild-type and HSF1 knockout control lines. As expected, we found that even in these cancer cells with high levels of HSF2 basal activity, HSF2 loss did not greatly alter the HSF1-dependent HSR (fig. S7, A and B). Thus, the increased HSF2 activity and concordant gene expression regulation by HSF2 and HSF1 in cancer highlight a role for HSF2 that is distinct from its dispensable nature in the HSR.

Cancer cells are not only subject to the stresses associated with rapid proliferation but also the stresses of the tumor microenvironment such as limited nutrient and oxygen availability. Because previous work established a role for HSF1 in nutrient and oxygen stress responses (*44*–*48*), we tested whether HSF2 might also have a role in these other malignancy-associated cellular stresses. To do so, we subjected control MDA-MB-231 cells or cells lacking HSF2, HSF1, or both to glycolytic stress with 2-deoxy-D-glucose (2-DG), serum starvation, or the hypoxia mimetic cobalt chloride ($CoCl_2$) (*49*) and performed RNA-seq. In stark contrast to cells subjected to thermal stress, loss of either or both HSFs resulted in similar and broadly dysregulated transcriptional responses to these stresses (Fig. 5, A, C, and E). *K*-means clustering under each condition revealed six major modules of gene expression regulation patterns: genes down-regulated by stress and either (i) up-regulated or (ii) further down-regulated by HSF loss, genes little changed in stress but either (iii) up-regulated or (iv) down-regulated with HSF loss, (v) genes increased with stress or HSF1 loss, but decreased with HSF2 loss, and (vi) genes up-regulated by stress that are further increased with HSF loss. This transcriptional dysregulation involved genes implicated in cell development and differentiation, adhesion, signaling, oxygen response, and proliferation and included many direct target genes. Select genes highlight distinct patterns of dysregulation (Fig. 5, B, D, and F). For example, both nutrient stresses induce *AHSA1*, a co-chaperone critical for HSP90 function, but cells that lack HSF1 induce *AHSA1* to a lesser extent and HSF2 knockout cells are unable to induce *AHSA1* altogether. Similar results are observed for *HSPH1*. The expression of another class of genes is induced to a similar degree when stress is applied but is already suppressed in the absence of HSF1 or HSF2 under control conditions. For example, despite induction with serum starvation for each genetic background, *LPIN1*, a gene critical for triglyceride synthesis and implicated in the pathogenesis of lipodystrophies (*50*), fails to increase in expression beyond basal levels in cells lacking HSF1 and HSF2. Some genes, such as *BMP4*, have lower basal levels of expression in the absence of HSF1 or HSF2 and decrease further with the addition of stress. Notably, HSF2 strongly represses a subset of directly bound genes including *EFEMP1* and *PROM2* (i.e.,

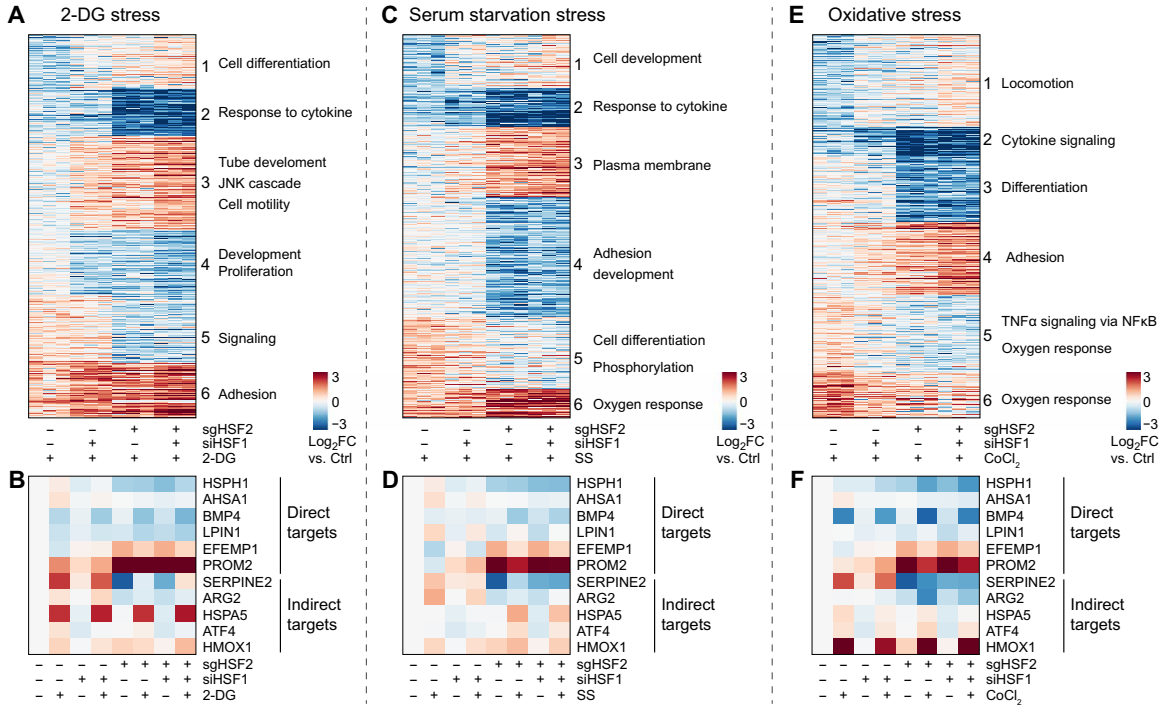

Fig. 5. HSF2 and HSF1 promote the transcriptional response to cancer-associated stresses. We treated HSF2 knockout (sgHSF2) or control (sgNT) MDA-MB-231 cells with siHSF1 or NT (siNT). Cells were treated with either 10 mM 2-DG for 24 hours, serum starvation (SS) for 48 hours, or 250 μM cobalt chloride ($CoCl_2$). (**A**, **C**, and **E**) Differentially expressed genes were determined relative to unstressed sgNT + siNT cells (Ctrl). Enriched GSEA terms are indicated. JNK, c-Jun N-terminal kinase. (**B**, **D**, and **F**) Select genes from (A) to (C) are plotted and labeled as direct or indirect transcriptional targets based on ChIP-seq from Fig. 2.

expression increased with loss). Still, many other genes are dysregulated indirectly (not bound in ChIP-seq, e.g., *SERPINE2* and *ARG2*), demonstrating a broader transcriptional rewiring that occurs because of long-term HSF2 loss and stress. These consequences of HSF2 loss and its similarity to HSF1 loss under conditions of impaired glycolysis, low serum, or oxygen deprivation highlight that while HSF2 and HSF1 have clearly divergent functions in response to thermal stress, they share a similar and pervasive role in regulating gene expression in cells subjected to these metabolic stresses.

HSF2 is required for tumor progression in cell line xenografts of prostate and breast cancer

Our results demonstrate that HSF2 interacts with HSF1 to bind and regulate a program of genes that support the anabolic state of many cancers, while also promoting the response to stresses that characterize the tumor microenvironment. However, how HSF2's function in regulating cancer cell transcription in vitro relates to tumorigenesis in vivo is not well understood. To address this question, we first injected our PC3M clonal knockouts or MDA-MB-231 population knockouts of HSF2 or HSF1 subcutaneously into immunocompromised [nonobese diabetic–*scid* IL2Rg^{null} (NSG)] mice and measured tumor volume over time and mouse survival. Knockout of HSF2 in the PC3M cell line resulted in a notable reduction in tumor growth compared to control (Fig. 6A), and these effects were indistinguishable from tumors resulting from HSF1 knockout cells. The reduced tumor growth corresponded to prolonged mouse survival (Fig. 6B). We obtained similar, although blunted, effects in the MDA-MB-231 cell line (Fig. 6, C and D).

To better understand these results, we excised and characterized the resultant tumors by immunohistochemistry (IHC) and RNA-seq. Notably, IHC staining for HSF1 in MDA-MB-231 tumors revealed heterogenous HSF1-positive staining (fig. S8A) that reflects a minority subpopulation of HSF1-expressing cells had grown out from the initial knockout population, despite immunoblot confirmation prior to injection (fig. S2F). This result suggests that the observed tumor growth reduction, while not statistically significant, is underestimated. Lower levels of HSF2 expression in MDA-MB-231 tumors precluded assessment by IHC. Consistent with outgrowth of a wild-type subpopulation of cells, very few genes were differentially expressed between control and knockout tumors (fig. S8B), which contrasts with the many gene expression differences of these lines detected in vitro (fig. S8C).

Persistent knockout of HSF1 or HSF2 was confirmed for tumors derived from PC3M clonal knockouts by IHC (Fig. 6E) and additionally revealed reduced HSF2 staining for HSF1 knockout tumors. Consistent with our in vitro data, RNA-seq of HSF2 knockout tumors had similar gene expression to HSF1 knockout tumors (Fig. 6F) with decreased expression of protein folding ($Q = 7.1 \times 10^{-29}$) and protein metabolism ($Q = 2.8 \times 10^{-04}$) genes in common for HSF1- and HSF2-knockout tumors. While these effects have been reported for HSF1, our data establish a significant role for HSF2 in regulating these processes in cancer. Comparing the in vitro and in vivo RNA-seq for PC3M reveals significant overlap despite expected differences due to the complex contribution of the tumor microenvironment to cancer cell gene expression. Enriched pathways for sgHSF1 comparisons include HSF1 activation/attenuation ($Q = 1.73 \times 10^{-15}$) and regulation of protein metabolic processes

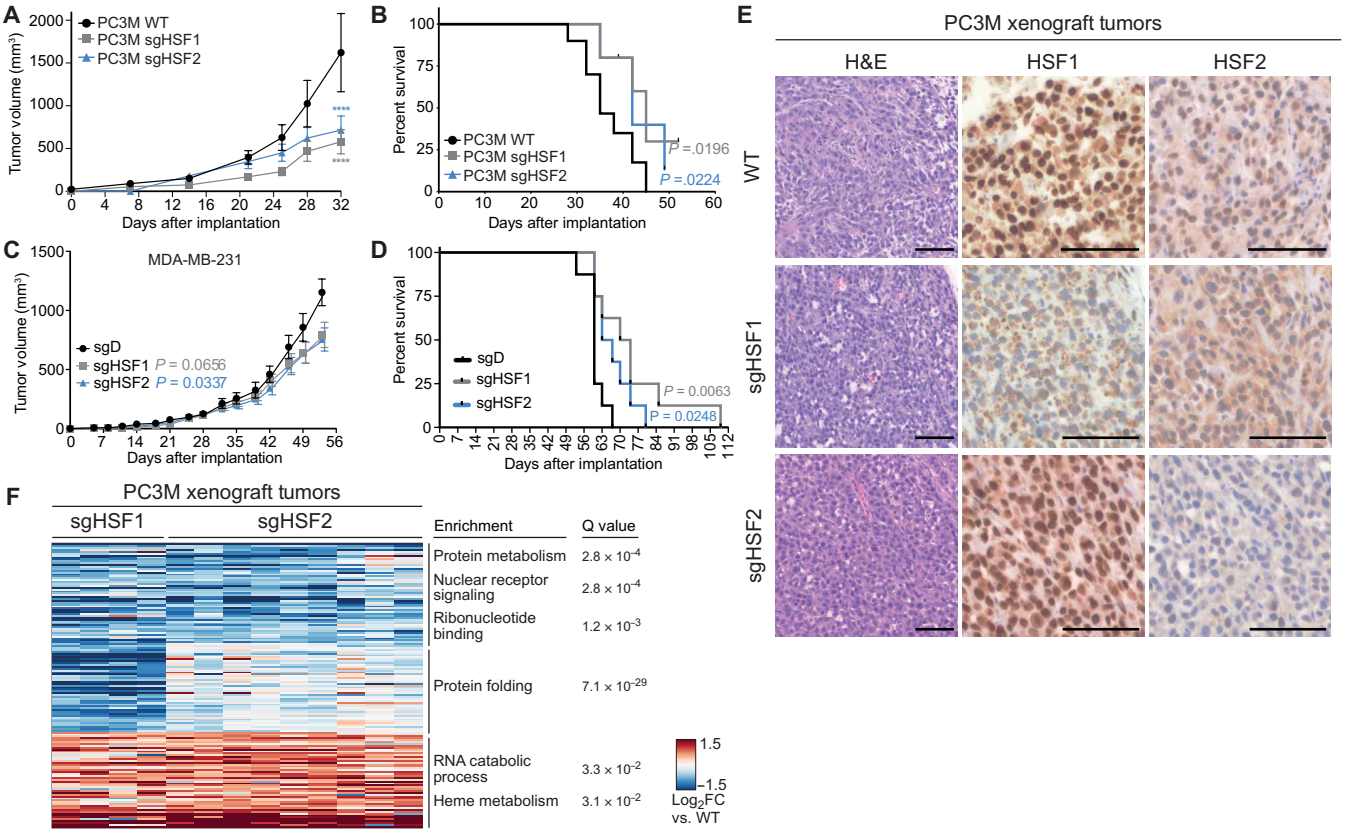

Fig. 6. HSF2 is required for tumor progression in cell line xenografts of prostate and breast cancer. (**A**) Tumor volume after subcutaneous injection of two independent PC3M cell clones for each of wild type, HSF1 knockout (sgHSF1), or HSF2 knockout (sgHSF2). Data are grouped by genotype, combined across clones. ****$P < 0.0001$ by two-way analysis of variance (ANOVA) at day 32 after inoculation. (**B**) Survival analysis of mice bearing PC3M tumors. (**C**) Tumor volume measurements for MDA-MB-231 xenografts. (**D**) Survival analysis for of mice bearing MDA-MB-231 tumors. (**E**) Representative hematoxylin and eosin (H&E) and IHC staining for HSF1 or HSF2 for PC3M cell line xenograft tumor. Scale bars, 100 μm. Immunoblot validation of knockout cells before injection are provided in fig. S2J. (**F**) RNA-seq performed on tumors from each knockout or control at experiment end point. Data are expressed as $\log_2$ fold change relative to four control tumors. Enriched GO terms are indicated.

($Q = 1.65 \times 10^{-14}$) (fig. S8D, left). The overlap for sgHSF2 is enriched for biological adhesion ($Q = 2.3 \times 10^{-3}$) and protein localization ($Q = 1.42 \times 10^{-2}$) (fig. S8D, right). Together, these data establish a critical role for HSF2 in directly regulating cancer gene expression programs, response to metabolic stresses, and tumor progression in cooperation with HSF1.

DISCUSSION

A large body of work has clearly established the importance of HSF1 activation across a diverse spectrum of cancers. HSF1 supports the malignant state by directing a transcriptional program of genes involved in many facets of tumorigenesis, extending far beyond protein folding and stress responses to include cell cycle, energy metabolism, and other proliferation-associated processes (*5*). High levels of HSF1 activation and its transcriptional activity correlate with metastasis and death in patients (*5*). Here, we establish that HSF2, similar to its paralog HSF1, is a significant contributor in supporting cancer cell gene expression programs.

Our data identify a prominent role for HSF2 in cancer where it cooperates with HSF1 in a manner that starkly contrasts with their divergent roles in the response to thermal stress. HSF1 has been well studied for its profound induction of chaperones upon acute heat stress and thus has served as a model for inducible gene expression, yielding significant insight into transcription regulation (*3*, *51*–*53*). Partly, because HSF2 does not play a significant role in promoting the response to heat stress (*2*, *4*, *43*, *54*), its role in transcription regulation—and biology in general—has been far less explored. For example, while HSF1 has an extensive body of literature connecting its activity to diseases that include cancer (*30*) and neurodegenerative diseases (*55*), among others (*2*), mechanistic studies of HSF2 biology are largely limited to its role in development and response to mild proteotoxic stresses (*56*). Here, we demonstrate that HSF2, similar to HSF1, promotes the expression of HSPs and non-HSP transcriptional targets to support the malignant state. Notably, these HSPs do not include those most inducible in response to elevated temperature, supporting the idea that studying HSF2 function at loci beyond the highly heat shock–inducible *HSP70* family and *HSP40* family genes will be critical to reveal a comprehensive picture of its role in regulating gene transcription.

Our study suggests that an important aspect of HSF1 function in cancer is to promote HSF2 abundance and activity, and phenotypes previously attributed solely to HSF1 may reflect the effect of loss of both HSFs. Thus, the effect of HSF1 loss on reducing HSF2 expression and chromatin occupancy may contribute to its more pronounced suppression of cell cycle and proliferation-associated gene expression.

On the other hand, it is possible that HSF2 loss alone falls below a threshold of cytotoxicity that fails to result in severe growth arrest because of the intact function of HSF1, explaining the greater absolute fitness cost of HSF1 loss versus HSF2 loss in large-scale genetic dependency screens (*35*). Because HSF1 has critical roles in many other aspects of biology (*30*, *56*), it will be important to understand the cooperation and interplay of HSF1 and HSF2 across diverse biological contexts.

Why might cancer cells engage both HSF1 and HSF2? Consistent with structural studies that have revealed highly conserved DNA binding domain conformations (*15*), our data demonstrate a nearly identical chromatin occupancy pattern of HSF1 and HSF2, suggesting that their specialization does not lie in DNA binding activity as has been described for other paralogous transcription factors (*57*). However, their divergence in surfaces that mediate protein-protein interactions could result in differential recruitment of regulatory cofactors. Considering HSF2 is a labile protein sensitive to rates of protein synthesis and degradation (*20*, *39*), another possibility is that it provides cancer cells an additional mechanism to meet the anabolic demands of proliferation and increased protein synthesis through the HSF cancer program. Proteins with a shorter half-life allow cells to rapidly adjust expression levels, and this regulatory feature can be observed in other proteins associated with proliferation (e.g., Myc). Meanwhile, cells maintain higher HSF1 levels, with a much longer half-life, to appropriately respond to sudden and acute proteotoxic stresses in addition to its cancer supporting functions. Other mechanisms, yet undiscovered, may also stabilize HSF2 during formation and maintenance of tumors. Lastly, previous observations that HSF2 has greater chromatin occupancy in mitotic cells than HSF1 (*58*) suggest that cell cycle–dependent differences between these paralogs ensure maintenance of these transcriptional programs in highly proliferative cells.

Our study also sheds light on the biological roots of the roles HSFs play in cancer. Previous work has revealed a notable similarity between HSF1's transcriptional program in cancer and that of the single HSF in *Caenorhabditis elegans* during larval development (*8*). Both cancer and larval development are characterized by biomass accumulation and cell proliferation generating increased demand on protein synthesis and quality control machinery. Each of these highly proliferative settings reveals an expansion of HSF1 transcriptional activity beyond its canonical HSR target genes to include anabolic gene expression programs. Considering the intimate link our study reveals between HSF2 and HSF1 in cancer and HSF2's more prominent role in development and mitotic gene expression regulation during mitosis (*58*, *59*), HSF2 may serve as a more direct connection between these developmental and proliferative gene expression programs. Thus, cancer cells seem to co-opt the ancient, developmental HSF program (*60*) to support the malignant state.

In conclusion, our study has documented a significant role for HSF2 in supporting malignancy. In contrast with heat shock, cancer-relevant stresses such as nutrient deprivation or in vivo tumorigenesis invoke an HSF2-driven gene expression program, which parallels that driven by HSF1. Thus, HSF2 is a critical HSF1 accomplice, promoting a gene expression program that supports the anabolic malignant state and fuels cancer progression.

MATERIALS AND METHODS

Cell culture

Cell lines were obtained from American Type Culture Collection or a gift from S. Lindquist. PC3M, NCI-H838, SKBR3, BT-20, ZR-75-1, HCC38, LNCaP, VCaP, and DLD1 cells were maintained in RPMI 1640 (Gibco, #11875119), 10% fetal bovine serum (Clontech, #631106), and 1% penicillin/streptomycin (pen/strep; Gibco, #15140122). MDA-MB-231, MCF7, MEFs, and 293T cells were maintained in Dulbecco's modified Eagle's medium (Gibco, #11995073), 10% fetal bovine serum, and 1% pen/strep. Cell lines were authenticated at the University of Arizona Genetics Core and tested negative for mycoplasma. Cells were lifted for passaging with Accumax (Innovative Cell Technologies, #AM105). Cells were maintained at 37°C and 5% CO_2 in a HeraCell Vios 160i incubator (Thermo Fisher Scientific).

MS and analysis

IP samples were prepared for LC-MS/MS with chloroform methanol precipitation (*61*). LC-MS/MS of immunoprecipitated GFP-Flag, HSF1-Flag, or HSF2-Flag was performed as described (*62*). Unfiltered MS data are available for experiment (see table S1). The following measurements and information are given for each protein identified: accession number, peptide count, NSAF (normalized spectral abundance factor), emPAI (exponentially modified protein abundance index), spectral count, percent sequence coverage, and description of protein identified. We defined high-confidence interacting proteins as those with at least threefold more spectral counts in our experiments relative to the average of spectral counts for affinity-purified MS from publicly available IP-MS experiments, specifically those targeting Flag epitope and agarose beads (crapome.org) (*63*).

LUMIER assay

The LUMIER assay was performed essentially as described previously (Taipale 2014). Briefly, 3X FLAG-tagged bait proteins (table S2) were transiently transfected in 96-well format into a 293T cell line stably expressing HSF1 with a codon-optimized *Renilla reniformis* luciferase C-terminal tag. Two days after transfection, cells were rapidly washed in 1× ice-cold phosphate-buffered saline (PBS) and lysed in ice-cold HENG buffer (50 mM HEPES-KOH pH 7.9, 150 mM NaCl, 2 mM EDTA, 5% glycerol, 0.5% Triton X-100 supplemented with protease, and phosphatase inhibitors) (Taipale 2012). The lysate was transferred into 384-well plates coated with monoclonal M2 antibody and blocked with 3% bovine serum albumin/5% sucrose/0.5% Tween 20. Plates were incubated at 4°C for 3 hours, after which plates were rapidly washed in HENG buffer. Last, luciferase-tagged HSF1 was detected by measuring luminescence using the Gaussia FLEX Luciferase Kit [New England Biolabs (NEB)]. An HSF1-LUMIER interaction score was determined from the $\log_2$-transformed bait-FLAG/GFP-FLAG luminescence ratio (reported in table S2).

Electrophoretic mobility shift assay

EMSAs were performed as described previously (*64*) with modifications based on the LICOR Odyssey EMSA kit protocol to accommodate the infrared dye (IRDye) labeling and detection strategy. EMSA protein lysates were prepared either from NCI-H838 cells or from $Hsf1^{+/+}$ or $Hsf1^{-/-}$ MEFs treated with either dimethyl sulfoxide control or 10 μM MG-132. Briefly, cells were washed twice with ice-cold PBS, scraped, centrifuged, flash-frozen, and stored at −80°C. The frozen cell pellets were lysed in buffer containing 20 mM tris (pH 8.0), 25% glycerol, 420 mM NaCl, 1.5 mM $MgCl_2$, 0.2 mM EDTA, 0.5 mM dithiothreitol (DTT), and protease inhibitor cocktail. Samples were centrifuged for 5 min at 100,000*g*, and supernatants were flash-frozen and stored at −80°C. Protein concentrations were determined using a BCA protein assay (Pierce).

EMSA DNA substrates were prepared as follows. All oligonucleotides were resuspended in 1× TE buffer [10 mM tris (pH 8.0) and 1 mM EDTA] to a final concentration of 20 pmol/μl. Then, 5 μl of forward and reverse oligonucleotides were mixed in a single tube as and annealed by placing in a 100°C heat block for 5 min, followed by turning of the heat block and allowing it to slowly cool to room temperature. A working DNA substrate stock was prepared by diluting annealed oligos (1:200) in water. Substrates were prepared that were labeled with DY-782 or DY-672 (where both forward and reverse oligos were end-labeled with the same IRDye) or where unlabeled for use as a cold competitor.

EMSA binding reactions were performed using 8 μg of lysates, 5 nM IRDye labeled oligo (see Table 1), 100 nM unlabeled competitor oligo, and 100 nM antibody or control IgG, as indicated in binding buffer containing 10 mM tris (pH 7.5), 1 mM EDTA, 100 mM NaCl, poly(deoxyinosinic-deoxycytidylic) (50 ng/μl), 0.5 mM DTT, and 0.25% Tween 20. Reactions were incubated for 20 min at room temperature after which 1 μl of 10× Orange loading dye (LI-COR, P/N 927-1010 0) was added to each reaction, mixed, and loaded on a Mini-PROTEAN TBE precast gel (Bio-Rad). The gel was run at 10 V/cm for about 30 min in 1× Tris/Borate/EDTA (TBE) buffer. Following electrophoresis, gels were imaged directly on an LI-COR Odyssey imager.

Immunoprecipitation

Cells were rinsed twice with cold PBS, removed from plates by scraping, and centrifuged for 4 min at 1000*g* and 4°C before pellet resuspension in cold lysis buffer. For IPs of HSF1 or HSF2, cells were lysed in buffer containing 1% NP-40, 100 mM NaCl, 50 mM tris (pH 7.5), 0.2 mM EDTA, 5% glycerol, and 1 mM phenylmethylsulfonyl fluoride (PMSF), and lysis was achieved by sonication in a 4°C water bath (10 cycles of 30-s on and 1-min off). After lysis, cells were spun at 21,000*g* at 4°C for 10 min, and the supernatant was kept for input and IP. FLAG-IPs were performed using M2 affinity agarose (Thermo Fisher Scientific). HSF1 IP was performed with a polyclonal rabbit anti-HSF1 antibody (Cell Signaling Technology, #4356S). HSF2 IP was performed with a monoclonal rat anti-HSF2 (3E2) antibody (Santa Cruz Biotechnology, sc-13517). As a control for nonspecific binding, normal mouse IgG was immunoprecipitated (Santa Cruz Biotechnology, sc-2027).

Immunoblot

Protein samples were lysed in radioimmunoprecipitation assay buffer [10 mM tris-Cl (pH 8.0), 1 mM EDTA, 0.5 mM EGTA, 1% Triton X-100, 0.1% sodium deoxycholate, 0.1% SDS, and 140 mM NaCl] containing 1 mM PMSF and a Roche cOmplete Protease Inhibitor Cocktail tablet (catalog no. 11697498001) and passed through a 21-gauge needle. Protein concentration was determined with a BCA assay (Pierce, #23255), denatured in Laemmli sample buffer containing 1% β-mercaptoethanol, and heated at 95C for 5 min. Electrophoresis used 4 to 20% bis-tris gradient gels unless otherwise specified, with transfer to polyvinylidene difluoride membranes using the iBlot 2 Dry Blotting System (Thermo Fisher Scientific). Membranes were blocked in 5% fat-free milk for 1 hour at room temperature. Primary and secondary antibodies were diluted in 5% fat free milk and exposed to membranes overnight at 4°C. Immunoblots were developed with Immobilon Western Chemiluminescent HRP Substrate (Millipore, #WBKLSO500) and visualized with a ChemiDoc Touch Imaging System (Bio-Rad, #732BR0783), and images were analyzed using ImageLab v6.0.1 (Bio-Rad). HSF1 immunoblot was performed with a polyclonal rabbit anti-HSF1 antibody (Cell Signaling Technology, #4356S). HSF2 immunoblot was performed with a monoclonal rat anti-HSF2 (3E2) antibody (Santa Cruz Biotechnology, sc-13517). Antibody specificity was confirmed with purified proteins. Equal loading of protein was confirmed with a β-actin monoclonal antibody (BA3R, Invitrogen, #MA5-15739).

Protein purification

Human HSF1 (NM_005526.4) and HSF2 (NM_004506.4) were cloned into the pET His6 MBP TEV LIC cloning vector that was a gift from S. Gradia (Addgene plasmid #29656) and verified by Sanger sequencing. BL21 DE3 (NEB) were transformed with either pHMH-HSF1 or pHMH-HSF2. A single colony was picked and incubated in 50 ml of LB broth in a shaking incubator overnight at 37°C. The next morning, the 50-ml cultures were diluted to 1 liter and incubated at 37°C until they were at an optical density (OD) of 0.5. At an OD of 0.5, protein production was induced with 1 mM isopropyl-β-D-thiogalactopyranoside (final concentration), and the cultures were incubated at 18°C overnight. Bacteria were harvested, resuspended in 30 ml of heparin binding buffer [50 mM Hepes (pH 7.4), 50 mM NaCl, 0.1 mM EDTA, and 5% glycerol] supplemented with lysozyme (10 μg/ml). Lysates were prepared by lysing the membranes with a sonicator (30% amplitude and 0.5-s on/off cycles for 2 min). The cellular debris was cleared by centrifugation (20,000*g* for 15 min at 4°C). The clear supernatant was passed through HiTrap heparin column (GE Healthcare) using ÄKTA high-performance LC system. The column was washed (10 column volumes) with heparin binding buffer and eluted over a linear salt gradient ranging from 50 to 1.5 M NaCl over 20 column volumes. Fractions from heparin elution were analyzed by SDS–polyacrylamide gel electrophoresis, followed by Coomassie staining. Appropriate fractions identified from this step were subject to Ni–NTA (nitrilotriacetic acid) (QIAGEN) purification as per the manufacturer's protocol. Briefly, heparin eluate was incubated with Ni-NTA resin for 2 hours on a shaker at 4°C, washed four times, and eluted with 250 mM

Table 1. Oligo sequences for EMSA experiments.

EMSA Oligo Name	EMSA Oligo Sequence (5′ to 3′)
EMSA-HSPA8-F	CTTATACCCTATCTTAGAACCTTCCAGAAGGGGCCCGCCC
EMSA-HSPA8-R	GGGCGGGCCCCTTCTGGAAGGTTCTAAGATAGGGTATAAG
EMSA-HSPA6-F	GGAAGGTGCGGGAAGGTGCGGAAAGGTTCGCGAAAGTTCG
EMSA-HSPA6-R	CGAACTTTCGCGAACCTTTCCGCACCTTCCCGCACCTTCC
EMSA-HSPA8*-F (mut HSE)	CTTATACCCTATCTTATAACCTTGCACAAGGGGCCCGCCC
EMSA-HSPA8*-R (mut HSE)	GGGCGGGCCCCTTGTGCAAGGTTATAAGATAGGGTATAAG

imidazole. Ni-NTA eluate proteins were resolved by gel filtration using a Superdex 200 10/300 GL column on ÄKTA system (GE Healthcare). Purified proteins were quantified by Nanodrop 2000 spectrophotometer (Thermo Fisher Scientific) and by the enhanced protocol for BCA Assay (Pierce, #23255). These purified recombinant proteins were used for confirming antibody specificity and quantitative immunoblot.

Quantitative immunoblot

For each cell line, 5×10^6 cells were plated in two 15-cm tissue culture dishes. Twenty-four hours later, one dish of cells was counted, and the second dish of cells was washed and scraped with cold PBS into a microfuge tube on ice. Cells were pelleted at 1000*g* for 5 min at 4°C. After discarding supernatant, cell pellets were snap-frozen in liquid nitrogen for 30 to 60 s and stored at −80°C. Subsequently, cell pellets were lysed as described above. Whole-cell extracts were loaded at two concentrations for each cell line alongside a standard curve of known amounts of recombinant HSF1 or HSF2. iBlot 2 was used to transfer protein to a nitrocellulose membrane. Membranes were blocked in Odyssey Blocking Buffer (LI-COR). Membranes were incubated in primary antibody (same as in immunoblot) at 4°C overnight in Odyssey Blocking Buffer plus 0.2% Tween 20 according to the manufacturer's protocol. Membranes were washed three times for 5 min with phosphate buffered saline with 0.1% Tween 20 (PBST) and then incubated in secondary antibody diluted in Odyssey Blocking Buffer plus 0.2% Tween 20 for 60 min at room temperature with LI-COR IRDye secondary antibodies at 1:5000 dilution: donkey anti-rabbit for detecting HSF1 (#926-32213) and goat anti-rat for detecting HSF2 (#926-68076). Membranes were washed with PBST and then rinsed in PBS to remove Tween 20. Membranes were imaged using the Odyssey CLx imager using autoexposure settings. Specific bands corresponding to the full-length proteins were quantified with Image Studio. Recombinant protein was used to generate a standard curve of known protein amount to LI-COR signal generating a linear model used to interpolate total target protein amount for each cell line. Because total protein was harvested from a known number of cells, we were able to calculate the number of molecules of HSF per cell.

HSF overexpression constructs

Overexpression constructs of HSF1 or HSF2 were generated by Gateway cloning HSF1 or HSF2 coding sequence in pLenti6.2-ccdB-3xFLAG-V5 that was a gift from M. Taipale (Addgene plasmid #87071) (*28*). MCF7 cells were subsequently selected with blasticidin. Expression of HSF1 and HSF2 was confirmed by immunoblot for either HSF or Flag.

Gene silencing

siGenome or ON-TARGET plus siRNA pools containing four gene-specific siRNAs were obtained for HSF1 and HSF2 (Dharmacon, Horizon Discovery), as well as an NT control siRNAs, and transfected using RNAiMAX (Thermo Fisher Scientific) according to the manufacturer's protocol. Unless otherwise specified, cells were harvested 72 hours after siRNA transfection. For serum starvation, serum was removed 48 hours after siRNA treatment and harvested after 48 hours of serum starvation. Knockdown was confirmed for each siRNA experiment by quantitative polymerase chain reaction (PCR)/RNA-seq or immunoblot.

CRISPR-Cas9 knockout generation

Unless otherwise noted, knockout cells were generated using CRISPR-Cas9 by introducing lentiCRISPRv2 with lentivirus (*65*, *66*). lentiCRISPRv2 was a gift from F. Zhang (Addgene plasmid #52961). Briefly, four sgRNAs sequences targeting HSF1 or HSF2 (see Table 2) were selected from the Brunello Human CRISPR Knockout Pooled Library (*67*) and cloned into lentiCRISPRv2 according to standard protocols. Lentiviral particles were produced using 293T cells transfected with lentiCRISPRv2, envelope plasmid (pMD2.G), and packaging plasmid (psPAX2). pMD2.G and psPAX2 were gifts from D. Trono (Addgene plasmid #12259 and #12260, respectively). Host cells were infected with lentivirus and final concentration of polybrene (8 μg/ml; MilliporeSigma, #TR-1003-G) and selected with puromycin (Sigma-Aldrich, P9620) for 2 to 4 days at an empirically determined concentration and duration for each cell line. Knockout populations were confirmed by immunoblot. For PC3M, we were unable to achieve population knockouts. Instead, clonal knockouts were generated by transducing with virus as described for populations. Single-cell clones were grown after fluorescence-activated cell sorting, and clonal knockouts were confirmed by Sanger sequencing and Western blot. Two clones of wild-type cell lines were also derived as controls. MDA-MB-231 dKO cells were generated through the two vector CRISPR-Cas9 system. Briefly, cells were infected and selected with sgRNA 1 (sgAAVS1 for all single knockouts and sgHSF2 for dKOs) in the lenti-guide-Puro vector (a gift from F. Zhang, plasmid #52963) lacking Cas9 so that cell editing would not yet begin. These cells were subsequently infected and selected with the second sgRNA cloned into the lenti-Cas9-Blast vector (a gift from F. Zhang, plasmid #52962). Control and single knockout cells received sgAAVS1 as a cutting control, and then the respective gRNAs were used in other cell lines (sgHSF1.1 or sgHSF2.1), with dKO cells receiving both HSF sgRNAs.

RNA harvesting, library prep, and sequencing

All reactions involving RNA were completed at an ribonuclease (RNase)–free bench. Cells were seeded in either 12-well or 6-well plates (two to three biological replicates). Cells were harvested with either TRIzol or Buffer RLT (QIAGEN) and then applied to Direct-zol (Zymo Research) or QIAGEN RNeasy Kit with deoxyribonuclease I on-column treatment according to the manufacturer's protocols (QIAGEN). RNA concentration and quality were determined using the Agilent 2100 Bioanalyzer or Agilent 4200 TapeStation according to the manufacturer's protocols. Samples with an RNA integrity number (RIN) greater than 7 were included in subsequent steps. Libraries were prepared from 100 ng of RNA using the Lexogen QuantSeq FWD Kit for Illumina sequencing using the Sciclone G3 NGS Workstation (PerkinElmer) according to the manufacturer's protocol, using 14 cycles of PCR library amplification. DNA Library quality and fragment size were assessed using Agilent High Sensitivity DNA kits for either the Agilent 2100 Bioanalyzer or Agilent 4200 TapeStation. Library concentrations were determined using the Qubit dsDNA HS assay

Table 2. sgRNA sequences for CRISPR-Cas9 knockout generation.

sgRNA Name	sgRNA sequence
sgHSF1.1	GCTCCAGCAGATGAGCGCGT
sgHSF2.1	CGGCTTTCCTCAGCAAGCTG
sgHSF1.2	CCGGCGGGAGCATAGACGAG
sgHSF2.2	TATGCACCTGTCATTCAGAG
sgAAVS1	GGGGCCACTAGGGACAGGAT

adapted to a 384-well format, scaling the reaction size down to 20 µl in triplicate (19 µl of working reagent and1 µl of sample or standard) with a series of 11 Qubit DNA standard dilutions (Invitrogen). Fluorescence was measured using a Tecan Infinite M1000 Pro plate reader (excitation, 480 nm; emission, 530 nm). Sequencing samples were pooled at equimolar amounts, diluted to a 4 nM final library concentration, denatured with 0.2 M NaOH (final concentration) for 5 min at room temperature, and quenched with 200 mM tris-HCl (pH 7). PhiX spike-in (1%) was used and libraries were run on an Illumina NextSeq or NovaSeq.

RNA-seq data processing and analysis

Raw Bcl files were converted to FASTQ using bcl2fastq software. Sequence quality was assessed with FastQC v0.11.2, FASTQ files were trimmed using BBduk from BBTools v35.92 according to Lexogen QuantSeq manufacturer's parameters, mapped to hg38 using STAR v2.6.0 and gene annotations from Ensembl 78. HTSeq was used to count uniquely mapped reads. Significantly differentially expressed genes were determined using EdgeR v3.26.8. A blocked experimental design analysis strategy was used (edgeR User's Guide, 3.4.2). This strategy limits inclusion of genes that are differentially expressed between different cell lines or cell type–specific siRNA treatment effects, thus emphasizing gene expression changes common to the treatment relative to control (siRNA versus siNT). This analysis was conducted independently for siHSF2 and siHSF1 and for each pool of siRNA hairpins. High-confidence differentially expressed genes were defined as the intersection of differentially expressed genes across siRNA pools for HSF2 or HSF1 to minimize inclusion of nonspecific gene expression changes. For the correlation analyses in Fig. 4B, fold change gene expression for the union of differentially expressed genes in any cell line was used.

Enriched gene ontology (GO) terms and *P* values were determined with the GSEA (*68*, *69*) using the Hallmark (H), Kyoto Encyclopedia of Genes and Genomes and Reactome (C2), GO biological process and molecular function (C5), and transcription factor targets in the Molecular Signatures Database (MSigDb; v7.2, msigdb.org). Analyses used Python v3.7.4, Pandas v0.25.1, Numpy v1.17.2, and data visualized with Seaborn v0.9.0 and Matplotlib 3.3.3.

ChIP-seq sample preparation and analysis

Cells were cross-linked with 1% formaldehyde for 10 min at room temperature, quenched with 0.125 M glycine (final concentration) for 5 min at room temperature, and washed twice with PBS. Cells were harvested with ice-cold PBS and pelleted at 1000*g* for 5 min at 4°C, flash-frozen in liquid nitrogen, and stored at −80°C before lysis and micrococcal nuclease (MNase) digestion. Cell pellets were lysed in ice-cold lysis buffer [1% SDS, 10 mM EDTA, 50 mM tris-HCl (pH 8), and 1× protease inhibitor] and gently shook for 10 min at 4°C. Cell suspensions were spun down at 1350*g* for 5 min at 4°C, supernatant discarded, and resuspended in ice-cold MNase digestion buffer [50 mM tris-HCl (pH 8), 5 mM $CaCl_2$, and 1× protease inhibitor]. MNase (ChIP grade, 100 U/µl) was diluted (1:10) with MNase digestion buffer, added to cell lysates, and incubated in a 37°C water bath for 30 min, mixing every 5 min. The reactions were quenched with 10 mM EDTA and 20 mM EGTA on ice for 5 min. Cell lysates were spun down at 1350*g* for 5 min at 4°C to recover nuclei. Cell nuclei were resuspended in 2 ml of ice-cold ChIP buffer [1% Triton X-100, 2 mM EDTA, 150 ml of NaCl, 20 mM tris-HCl (pH 8), 3 mM $CaCl_2$, and 1× protease inhibitor] and sonicated with 800 mg of sonication beads for five cycles of 30-s on/off. Sonicated lysates were recovered and spun down at high speed for 10 min at 4°C. Sheared chromatin (10%) was saved as an input, and the rest was incubated with Dynabeads Protein G magnetic beads (Thermo Fisher Scientific, catalog no. 10009D) containing HSF1 antibody validated previously (*5*) (Santa Cruz Biotechnology, H-311) or HSF2 antibody (3E2, Santa Cruz Biotechnology) and rotated at 4°C overnight. Wash steps were conducted as detailed previously (*70*). HSF-bound beads were recovered using magnetic particle concentrator, washed once with 1 ml of wash buffer B [20 mM tris-HCl (pH 8), 150 mM NaCl, 2 mM EDTA (pH 8), 0.1% SDS, and 1% Triton X-100], washed once with buffer C [20 mM tris-HCl (pH 8), 500 mM NaCl, 2 mM EDTA (pH 8), 0.1% SDS, and 1% Triton X-100], once with buffer D [10 mM tris-HCl (pH 8), 250 mM LiCl, 1 mM EDTA (pH 8), 1% Na-deoxycholate, and 1% IGEPAL CA-360], and once with buffer TE [10 mM tris-HCl (pH 8), 1 mM EDTA (pH 8), and 50 mM NaCl], discarding the supernatant each wash. Beads were spun down at 1000*g* for 3 min at 4°C to remove any residual TE buffer. Chromatin-protein complexes and 10% inputs were extracted and decross-linked with 300 µl of extraction buffer (20 mM tris-HCl, 10 mM EDTA, 5 mM EGTA, 1% SDS, 300 mM NaCl, and proteinase K) at 65°C overnight. Samples were cooled to room temperature and vortexed, and proteinase K was inactivated with an incubation at 95°C for 10 min. Beads were collected and eluted, and decross-linked chromatin was recovered. Chromatin was incubated with RNase A at final concentration (0.2 mg/ml) at 37°C for 2 hours. Fragmented DNA was purified with Zymo Research ChIP DNA concentrator kit. Preparation of the ChIP-seq DNA library was performed with KAPA HTP library preparation kit (Roche, KK8234) and sequenced on an Illumina NextSeq as described above. Reads were aligned to hg38 using Bowtie v0.12.9. Peaks were called relative to knockout samples using MACS v1.4.2 and annotated from Ensembl 78. Heatmaps and metaplots were created using NGS plots. ChIP tracks were visualized using UCSC Genome Browser. Relative ChIP binding alongside RNA-seq data represents average peak intensity for MDA-MB-231 and PC3M experiments. Binding for each gene is plotted as a percentage of the maximum peak for each HSF to account for differences in antibody binding intensity. The scale max is set at 10 to aid visualization of intermediate peak intensities.

Coessentiality analysis

Gene essentiality data derived from CRISPR-Cas9 genome-scale loss-of-function screening of 739 cancer cell lines (*35*) using a modified Avana library (*67*) as part of Project Achilles were obtained from the Broad Institute's DepMap portal (20q1 release). Data were downloaded from https://depmap.org/portal/download/. Locus-adjusted gene coessentiality was determined as described previously (*36*) and implemented at fireworks.mendillolab.org. Briefly, the dependency score for each gene is corrected using a sliding window approach that minimizes bias at genomic regions, which have variable copy number across cell lines. Then, all possible gene-gene correlations are assessed and ranked by Pearson correlation coefficient. Highly ranked correlations indicate similar contextual essentiality and imply functional importance in the same pathway(s).

Xenograft experiments and analysis

MDA-MB-231 population knockouts or PC3M clonal knockouts and their respective controls were engineered to express pUltra-Chili-Luciferase (Addgene plasmid #48688). NSG mice were obtained

from the Jackson Laboratory, female mice were used for MDA-MB-231 breast cancer experiments, and male mice were used for PC3M prostate cancer experiments. Cells were suspended in PBS and Matrigel (50:50), and 5×10^6 cells per mouse were injected into the right mammary fat pad in a volume of 0.05 ml. Eight mice were inoculated for each genetic group (e.g., HSF1 knockout, sgNT control) for each cell line. Body weight and tumor volume were measured using calipers twice per week. Mice were euthanized when tumor volume reached 1500 mm^3. A repeated-measures analysis of variance (ANOVA) was conducted using GraphPad Prism 9 with Dunnett's multiple comparison test corrections. Significance was considered $\alpha < 0.05$. Survival analyses were conducted with a log-rank Mantel-Cox test in GraphPad Prism 9. No significant differences were observed for body weight in either experiment. Data are plotted as a summary of all eight mice of the same knockout status. All animal experiments were performed according to Institutional Animal Care and Use Committee–approved protocols.

Xenograft RNA-seq and analysis

A slice of flash-frozen tumors (no more than 30 mg) was lysed according to the manufacturer's protocol with a rotor-stator homogenizer using the RNeasy Kit (QIAGEN). One section from each of four independent tumors of similar size at time of experiment termination was used. RNA quantity and quality were determined as above. NEBNext Ultra II DNA Library Prep Kit for Illumina was used according to the manufacturer's protocol (NEB #E7103) and sequenced as described above. Where necessary, reads mapping better to mouse than human genomes were removed using Disambiguate software package using the Python implementation (*71*). Samples containing too few reads mapped to the human genome were removed from the analysis that included one MDA-MB-231 sgNT and two PC3Mc2 sgHSF2 tumor samples.

SUPPLEMENTARY MATERIALS

Supplementary material for this article is available at https://science.org/doi/10.1126/sciadv.abj6526

View/request a protocol for this paper from *Bio-protocol*.

REFERENCES AND NOTES

1. S. Lindquist, The heat-shock response. *Annu. Rev. Biochem.* **55**, 1151–1191 (1986).
2. R. Gomez-Pastor, E. T. Burchfiel, D. J. Thiele, Regulation of heat shock transcription factors and their roles in physiology and disease. *Nat. Rev. Mol. Cell Biol.* **19**, 4–19 (2018).
3. A. Vihervaara, F. M. Duarte, J. T. Lis, Molecular mechanisms driving transcriptional stress responses. *Nat. Rev. Genet.* **19**, 385–397 (2018).
4. D. B. Mahat, H. H. Salamanca, F. M. Duarte, C. G. Danko, J. T. Lis, Mammalian heat shock response and mechanisms underlying its genome-wide transcriptional regulation. *Mol. Cell* **62**, 63–78 (2016).
5. M. L. Mendillo, S. Santagata, M. Koeva, G. W. Bell, R. Hu, R. M. Tamimi, E. Fraenkel, T. A. Ince, L. Whitesell, S. Lindquist, HSF1 drives a transcriptional program distinct from heat shock to support highly malignant human cancers. *Cell* **150**, 549–562 (2012).
6. S. Santagata, M. L. Mendillo, Y. C. Tang, A. Subramanian, C. C. Perley, S. P. Roche, B. Wong, R. Narayan, H. Kwon, M. Koeva, A. Amon, T. R. Golub, J. A. Porco Jr., L. Whitesell, S. Lindquist, Tight coordination of protein translation and HSF1 activation supports the anabolic malignant state. *Science* **341**, 1238303 (2013).
7. R. Scherz-Shouval, S. Santagata, M. L. Mendillo, L. M. Sholl, I. Ben-Aharon, A. H. Beck, D. Dias-Santagata, M. Koeva, S. M. Stemmer, L. Whitesell, S. Lindquist, The reprogramming of tumor stroma by HSF1 is a potent enabler of malignancy. *Cell* **158**, 564–578 (2014).
8. J. Li, L. Chauve, G. Phelps, R. M. Brielmann, R. I. Morimoto, E2F coregulates an essential HSF developmental program that is distinct from the heat-shock response. *Genes Dev.* **30**, 2062–2075 (2016).
9. C. M. Filone, I. S. Caballero, K. Dower, M. L. Mendillo, G. S. Cowley, S. Santagata, D. K. Rozelle, J. Yen, K. H. Rubins, N. Hacohen, D. E. Root, L. E. Hensley, J. Connor, The master regulator of the cellular stress response (HSF1) is critical for orthopoxvirus infection. *PLOS Pathog.* **10**, e1003904 (2014).
10. S. Santagata, R. Hu, N. U. Lin, M. L. Mendillo, L. C. Collins, S. E. Hankinson, S. J. Schnitt, L. Whitesell, R. M. Tamimi, S. Lindquist, T. A. Ince, High levels of nuclear heat-shock factor 1 (HSF1) are associated with poor prognosis in breast cancer. *Proc. Natl. Acad. Sci. U.S.A.* **108**, 18378–18383 (2011).
11. K. D. Sarge, S. P. Murphy, R. I. Morimoto, Activation of heat shock gene transcription by heat shock factor 1 involves oligomerization, acquisition of DNA-binding activity, and nuclear localization and can occur in the absence of stress. *Mol. Cell. Biol.* **13**, 1392–1407 (1993).
12. L. Sistonen, K. D. Sarge, B. Phillips, K. Abravaya, R. I. Morimoto, Activation of heat shock factor 2 during hemin-induced differentiation of human erythroleukemia cells. *Mol. Cell. Biol.* **12**, 4104–4111 (1992).
13. L. Sistonen, K. D. Sarge, R. I. Morimoto, Human heat shock factors 1 and 2 are differentially activated and can synergistically induce hsp70 gene transcription. *Mol. Cell. Biol.* **14**, 2087–2099 (1994).
14. A. Mathew, S. K. Mathur, C. Jolly, S. G. Fox, S. Kim, R. I. Morimoto, Stress-specific activation and repression of heat shock factors 1 and 2. *Mol. Cell. Biol.* **21**, 7163–7171 (2001).
15. A. M. Jaeger, C. W. Pemble IV, L. Sistonen, D. J. Thiele, Structures of HSF2 reveal mechanisms for differential regulation of human heat-shock factors. *Nat. Struct. Mol. Biol.* **23**, 147–154 (2016).
16. A. Sandqvist, J. K. Björk, M. Åkerfelt, Z. Chitikova, A. Grichine, C. Vourc'h, C. Jolly, T. A. Salminen, Y. Nymalm, L. Sistonen, Heterotrimerization of heat-shock factors 1 and 2 provides a transcriptional switch in response to distinct stimuli. *Mol. Biol. Cell* **20**, 1340–1347 (2009).
17. G. Wang, Z. Ying, X. Jin, N. Tu, Y. Zhang, M. Phillips, D. Moskophidis, N. F. Mivechi, Essential requirement for both hsf1 and hsf2 transcriptional activity in spermatogenesis and male fertility. *Genesis* **38**, 66–80 (2004).
18. W. Widlak, N. Vydra, The role of heat shock factors in mammalian spermatogenesis. *Adv. Anat. Embryol. Cell Biol.* **222**, 45–65 (2017).
19. J. Joutsen, A. J. Da Silva, J. C. Luoto, M. A. Budzynski, A. S. Nylund, A. de Thonel, J.-P. Concordet, V. Mezger, D. Sabéran-Djoneidi, E. Henriksson, L. Sistonen, Heat shock factor 2 protects against proteotoxicity by maintaining cell-cell adhesion. *Cell Rep.* **30**, 583–597.e6 (2020).
20. A. Mathew, S. K. Mathur, R. I. Morimoto, Heat shock response and protein degradation: Regulation of HSF2 by the ubiquitin-proteasome pathway. *Mol. Cell. Biol.* **18**, 5091–5098 (1998).
21. T. Shinkawa, K. Tan, M. Fujimoto, N. Hayashida, K. Yamamoto, E. Takaki, R. Takii, R. Prakasam, S. Inouye, V. Mezger, A. Nakai, Heat shock factor 2 is required for maintaining proteostasis against febrile-range thermal stress and polyglutamine aggregation. *Mol. Biol. Cell* **22**, 3571–3583 (2011).
22. R. E. Fatimy, F. Miozzo, A. L. Mouël, R. Abane, L. Schwendimann, D. Sabéran-Djoneidi, A. de Thonel, I. Massaoudi, L. Paslaru, K. Hashimoto-Torii, E. Christians, P. Rakic, P. Gressens, V. Mezger, Heat shock factor 2 is a stress-responsive mediator of neuronal migration defects in models of fetal alcohol syndrome. *EMBO Mol. Med.* **6**, 1043–1061 (2014).
23. J. K. Björk, M. Åkerfelt, J. Joutsen, M. C. Puustinen, F. Cheng, L. Sistonen, M. Nees, Heat-shock factor 2 is a suppressor of prostate cancer invasion. *Oncogene* **35**, 1770–1784 (2016).
24. W. Zhong, J. S. Myers, F. Wang, K. Wang, J. Lucas, E. Rosfjord, J. Lucas, A. T. Hooper, S. Yang, L. A. Lemon, M. Guffroy, C. May, J. R. Bienkowska, P. A. Rejto, Comparison of the molecular and cellular phenotypes of common mouse syngeneic models with human tumors. *BMC Genomics* **21**, 2 (2020).
25. X. Meng, X. Chen, P. Lu, W. Ma, D. Yue, L. Song, Q. Fan, miR-202 promotes cell apoptosis in esophageal squamous cell carcinoma by targeting HSF2. *Oncol. Res.* **25**, 215–223 (2017).
26. P. Roos-Mattjus, L. Sistonen, Interplay between mammalian heat shock factors 1 and 2 in physiology and pathology. *FEBS J.* (2021).
27. M. C. Puustinen, L. Sistonen, Molecular mechanisms of heat shock factors in cancer. *Cell* **9**, (2020).
28. M. Taipale, G. Tucker, J. Peng, I. Krykbaeva, Z. Y. Lin, B. Larsen, H. Choi, B. Berger, A. C. Gingras, S. Lindquist, A quantitative chaperone interaction network reveals the architecture of cellular protein homeostasis pathways. *Cell* **158**, 434–448 (2014).
29. M. Taipale, I. Krykbaeva, M. Koeva, C. Kayatekin, K. D. Westover, G. I. Karras, S. Lindquist, Quantitative analysis of HSP90-client interactions reveals principles of substrate recognition. *Cell* **150**, 987–1001 (2012).
30. M. J. Alasady, M. L. Mendillo, The multifaceted role of HSF1 in tumorigenesis. *Adv. Exp. Med. Biol.* **1243**, 69–85 (2020).
31. D. Pincus, Regulation of Hsf1 and the heat shock response. *Adv. Exp. Med. Biol.* **1243**, 41–50 (2020).
32. J. Pan, R. M. Meyers, B. C. Michel, N. Mashtalir, A. E. Sizemore, J. N. Wells, S. H. Cassel, F. Vazquez, B. A. Weir, W. C. Hahn, J. A. Marsh, A. Tsherniak, C. Kadoch, Interrogation

of mammalian protein complex structure, function, and membership using genome-scale fitness screens. *Cell Syst.* **6**, 555–568.e7 (2018).
33. C. Boone, H. Bussey, B. J. Andrews, Exploring genetic interactions and networks with yeast. *Nat. Rev. Genet.* **8**, 437–449 (2007).
34. T. Wang, H. Yu, N. W. Hughes, B. Liu, A. Kendirli, K. Klein, W. W. Chen, E. S. Lander, D. M. Sabatini, Gene essentiality profiling reveals gene networks and synthetic lethal interactions with oncogenic ras. *Cell* **168**, 890–903.e15 (2017).
35. R. M. Meyers, J. G. Bryan, J. M. McFarland, B. A. Weir, A. E. Sizemore, H. Xu, N. V. Dharia, P. G. Montgomery, G. S. Cowley, S. Pantel, A. Goodale, Y. Lee, L. D. Ali, G. Jiang, R. Lubonja, W. F. Harrington, M. Strickland, T. Wu, D. C. Hawes, V. A. Zhivich, M. R. Wyatt, Z. Kalani, J. J. Chang, M. Okamoto, K. Stegmaier, T. R. Golub, J. S. Boehm, F. Vazquez, D. E. Root, W. C. Hahn, A. Tsherniak, Computational correction of copy number effect improves specificity of CRISPR-Cas9 essentiality screens in cancer cells. *Nat. Genet.* **49**, 1779–1784 (2017).
36. D. R. Amici, J. M. Jackson, M. I. Truica, R. S. Smith, S. A. Abdulkadir, M. L. Mendillo, FIREWORKS: A bottom-up approach to integrative coessentiality network analysis. *Life Sci. Alliance* **4**, e202000882 (2021).
37. A. Tsherniak, F. Vazquez, P. G. Montgomery, B. A. Weir, G. Kryukov, G. S. Cowley, S. Gill, W. F. Harrington, S. Pantel, J. M. Krill-Burger, R. M. Meyers, L. Ali, A. Goodale, Y. Lee, G. Jiang, J. Hsiao, W. F. J. Gerath, S. Howell, E. Merkel, M. Ghandi, L. A. Garraway, D. E. Root, T. R. Golub, J. S. Boehm, W. C. Hahn, Defining a cancer dependency map. *Cell* **170**, 564–576.e16 (2017).
38. P. Ostling, J. K. Bjork, P. Roos-Mattjus, V. Mezger, L. Sistonen, Heat shock factor 2 (HSF2) contributes to inducible expression of hsp genes through interplay with HSF1. *J. Biol. Chem.* **282**, 7077–7086 (2007).
39. S. Santopolo, A. Riccio, A. Rossi, M. G. Santoro, The proteostasis guardian HSF1 directs the transcription of its paralog and interactor HSF2 during proteasome dysfunction. *Cell. Mol. Life Sci.* **78**, 1113–1129 (2021).
40. R. M. Neve, K. Chin, J. Fridlyand, J. Yeh, F. L. Baehner, T. Fevr, L. Clark, N. Bayani, J. P. Coppe, F. Tong, T. Speed, P. T. Spellman, S. DeVries, A. Lapuk, N. J. Wang, W. L. Kuo, J. L. Stilwell, D. Pinkel, D. G. Albertson, F. M. Waldman, F. McCormick, R. B. Dickson, M. D. Johnson, M. Lippman, S. Ethier, A. Gazdar, J. W. Gray, A collection of breast cancer cell lines for the study of functionally distinct cancer subtypes. *Cancer Cell* **10**, 515–527 (2006).
41. C. Dai, L. Whitesell, A. B. Rogers, S. Lindquist, Heat shock factor 1 is a powerful multifaceted modifier of carcinogenesis. *Cell* **130**, 1005–1018 (2007).
42. N. Kourtis, C. Lazaris, K. Hockemeyer, J. C. Balandrán, A. R. Jimenez, J. Mullenders, Y. Gong, T. Trimarchi, K. Bhatt, H. Hu, L. Shrestha, A. Ambesi-Impiombato, M. Kelliher, E. Paietta, G. Chiosis, M. L. Guzman, A. A. Ferrando, A. Tsirigos, I. Aifantis, Oncogenic hijacking of the stress response machinery in T cell acute lymphoblastic leukemia. *Nat. Med.* **24**, 1157–1166 (2018).
43. E. J. Solís, J. P. Pandey, X. Zheng, D. X. Jin, P. B. Gupta, E. M. Airoldi, D. Pincus, V. Denic, Defining the essential function of yeast hsf1 reveals a compact transcriptional program for maintaining eukaryotic proteostasis. *Mol. Cell* **63**, 60–71 (2016).
44. X. Jin, D. Moskophidis, N. F. Mivechi, Heat shock transcription factor 1 is a key determinant of HCC development by regulating hepatic steatosis and metabolic syndrome. *Cell Metab.* **14**, 91–103 (2011).
45. K. H. Su, S. Dai, Z. Tang, M. Xu, C. Dai, Heat shock factor 1 is a direct antagonist of AMP-activated protein kinase. *Mol. Cell* **76**, 546–561.e8 (2019).
46. A. Qiao, X. Jin, J. Pang, D. Moskophidis, N. F. Mivechi, The transcriptional regulator of the chaperone response HSF1 controls hepatic bioenergetics and protein homeostasis. *J. Cell Biol.* **216**, 723–741 (2017).
47. Y. Zou, W. Zhu, M. Sakamoto, Y. Qin, H. Akazawa, H. Toko, M. Mizukami, N. Takeda, T. Minamino, H. Takano, T. Nagai, A. Nakai, I. Komuro, Heat shock transcription factor 1 protects cardiomyocytes from ischemia/reperfusion injury. *Circulation* **108**, 3024–3030 (2003).
48. C. Bierkamp, M. Luxey, A. Metchat, C. Audouard, R. Dumollard, E. Christians, Lack of maternal heat shock factor 1 results in multiple cellular and developmental defects, including mitochondrial damage and altered redox homeostasis, and leads to reduced survival of mammalian oocytes and embryos. *Dev. Biol.* **339**, 338–353 (2010).
49. J. Munoz-Sanchez, M. E. Chanez-Cardenas, The use of cobalt chloride as a chemical hypoxia model. *J. Appl. Toxicol.* **39**, 556–570 (2019).
50. M. Peterfy, J. Phan, P. Xu, K. Reue, Lipodystrophy in the fld mouse results from mutation of a new gene encoding a nuclear protein, lipin. *Nat. Genet.* **27**, 121–124 (2001).
51. M. J. Guertin, J. T. Lis, Chromatin landscape dictates HSF binding to target DNA elements. *PLOS Genet.* **6**, e1001114 (2010).
52. S. S. Teves, S. Henikoff, The heat shock response: A case study of chromatin dynamics in gene regulation. *Biochem. Cell Biol.* **91**, 42–48 (2013).
53. A. Vihervaara, D. B. Mahat, M. J. Guertin, T. Chu, C. G. Danko, J. T. Lis, L. Sistonen, Transcriptional response to stress is pre-wired by promoter and enhancer architecture. *Nat. Commun.* **8**, 255 (2017).
54. J. Korfanty, T. Stokowy, P. Widlak, A. Gogler-Piglowska, L. Handschuh, J. Podkowiński, N. Vydra, A. Naumowicz, A. Toma-Jonik, W. Widlak, Crosstalk between HSF1 and HSF2 during the heat shock response in mouse testes. *Int. J. Biochem. Cell Biol.* **57**, 76–83 (2014).
55. D. W. Neef, A. M. Jaeger, D. J. Thiele, Heat shock transcription factor 1 as a therapeutic target in neurodegenerative diseases. *Nat. Rev. Drug Discov.* **10**, 930–944 (2011).
56. M. Akerfelt, R. I. Morimoto, L. Sistonen, Heat shock factors: Integrators of cell stress, development and lifespan. *Nat. Rev. Mol. Cell Biol.* **11**, 545–555 (2010).
57. J. M. Rogers, M. L. Bulyk, Diversification of transcription factor-DNA interactions and the evolution of gene regulatory networks. *Wiley Interdiscip. Rev. Syst. Biol. Med.* **10**, e1423 (2018).
58. A. Vihervaara, C. Sergelius, J. Vasara, M. A. H. Blom, A. N. Elsing, P. Roos-Mattjus, L. Sistonen, Transcriptional response to stress in the dynamic chromatin environment of cycling and mitotic cells. *Proc. Natl. Acad. Sci. U.S.A.* **110**, E3388–E3397 (2013).
59. H. Xing, D. C. Wilkerson, C. N. Mayhew, E. J. Lubert, H. S. Skaggs, M. L. Goodson, Y. Hong, O. K. Park-Sarge, K. D. Sarge, Mechanism ofhsp70iGene bookmarking. *Science* **307**, 421–423 (2005).
60. J. Li, J. Labbadia, R. I. Morimoto, Rethinking HSF1 in stress, development, and organismal health. *Trends Cell Biol.* **27**, 895–905 (2017).
61. D. Wessel, U. I. Flugge, A method for the quantitative recovery of protein in dilute solution in the presence of detergents and lipids. *Anal. Biochem.* **138**, 141–143 (1984).
62. A. E. Hickox, A. C. Y. Wong, K. Pak, C. Strojny, M. Ramirez, J. R. Yates III, A. F. Ryan, J. N. Savas, Global analysis of protein expression of inner ear hair cells. *J. Neurosci.* **37**, 1320–1339 (2017).
63. D. Mellacheruvu, Z. Wright, A. L. Couzens, J. P. Lambert, N. A. St-Denis, T. Li, Y. V. Miteva, S. Hauri, M. E. Sardiu, T. Y. Low, V. A. Halim, R. D. Bagshaw, N. C. Hubner, A. al-Hakim, A. Bouchard, D. Faubert, D. Fermin, W. H. Dunham, M. Goudreault, Z. Y. Lin, B. G. Badillo, T. Pawson, D. Durocher, B. Coulombe, R. Aebersold, G. Superti-Furga, J. Colinge, A. J. R. Heck, H. Choi, M. Gstaiger, S. Mohammed, I. M. Cristea, K. L. Bennett, M. P. Washburn, B. Raught, R. M. Ewing, A. C. Gingras, A. I. Nesvizhskii, The CRAPome: A contaminant repository for affinity purification-mass spectrometry data. *Nat. Methods* **10**, 730–736 (2013).
64. D. D. Mosser, N. G. Theodorakis, R. I. Morimoto, Coordinate changes in heat shock element-binding activity and HSP70 gene transcription rates in human cells. *Mol. Cell. Biol.* **8**, 4736–4744 (1988).
65. O. Shalem, N. E. Sanjana, E. Hartenian, X. Shi, D. A. Scott, T. S. Mikkelsen, D. Heckl, B. L. Ebert, D. E. Root, J. G. Doench, F. Zhang, Genome-scale CRISPR-Cas9 knockout screening in human cells. *Science* **343**, 84–87 (2014).
66. N. E. Sanjana, O. Shalem, F. Zhang, Improved vectors and genome-wide libraries for CRISPR screening. *Nat. Methods* **11**, 783–784 (2014).
67. J. G. Doench, N. Fusi, M. Sullender, M. Hegde, E. W. Vaimberg, K. F. Donovan, I. Smith, Z. Tothova, C. Wilen, R. Orchard, H. W. Virgin, J. Listgarten, D. E. Root, Optimized sgRNA design to maximize activity and minimize off-target effects of CRISPR-Cas9. *Nat. Biotechnol.* **34**, 184–191 (2016).
68. A. Liberzon, C. Birger, H. Thorvaldsdóttir, M. Ghandi, J. P. Mesirov, P. Tamayo, The Molecular Signatures Database (MSigDB) hallmark gene set collection. *Cell Syst.* **1**, 417–425 (2015).
69. A. Subramanian, P. Tamayo, V. K. Mootha, S. Mukherjee, B. L. Ebert, M. A. Gillette, A. Paulovich, S. L. Pomeroy, T. R. Golub, E. S. Lander, J. P. Mesirov, Gene set enrichment analysis: A knowledge-based approach for interpreting genome-wide expression profiles. *Proc. Natl. Acad. Sci. U.S.A.* **102**, 15545–15550 (2005).
70. T. I. Lee, S. E. Johnstone, R. A. Young, Chromatin immunoprecipitation and microarray-based analysis of protein location. *Nat. Protoc.* **1**, 729–748 (2006).
71. M. J. Ahdesmaki, S. R. Gray, J. H. Johnson, Z. Lai, Disambiguate: An open-source application for disambiguating two species in next generation sequencing data from grafted samples. *F1000Res.* **5**, 2741 (2016).

Acknowledgments: We thank the members of the Mendillo Laboratory and the Department of Biochemistry and Molecular Genetics for suggestions and feedback. We thank E. Bartom for support in data analysis and sequencing data pipelines (https://github.com/ebartom/NGSbartom). We thank S. Marshall and E. Rendleman for assistance with sequencing. We thank A. L. George for use of the Odyssey CLx Imager for quantitative immunoblots. We thank the Developmental Therapeutics Core at Northwestern University Feinberg School of Medicine for conducting xenograft experiments. **Funding:** We would like to thank the ARCS Foundation Illinois Chapter for support of R.S.S. with an ARCS Scholar Award. R.S.S. was supported in part by the NIH (T32GM008152). M.L.M. was supported by the National Cancer Institute of the NIH (R00CA175293) and the Susan G. Komen Foundation (CCR17488145). M.L.M. was also supported by Kimmel Scholar (SKF-16-135) and Lynn Sage Scholar awards. HSR research in the Savas laboratory is supported by W81XWH-19-1-0627. D.R.A. was supported by the NIH (F30CA264513 and T32GM008152). M.J.A. was supported by the NIH (T32CA070085). **Author contributions:** R.S.S., S.R.T., S.S., L.W., S.L., and M.L.M.

conceptualized the project and designed the experiments. R.S.S., S.R.T., K.M., Y.W., and S.B. engineered cell lines. S.G. purified recombinant proteins. N.K. and J.N.S. performed MS. M.L.M. performed EMSA, and M.L.M. and M.T. performed LUMIER. All other experiments were performed by R.S.S., S.R.T., K.M., M.J.A., and S.L.T. R.S.S., D.R.A., S.R.T., and M.J.A. wrote code for implementing data analysis. D.R.A. performed coessentiality analysis. R.S.S. and M.L.M. wrote and revised the manuscript. M.L.M. supervised the project. **Competing interests:** The authors declare that they have no competing interests. **Data and materials availability:** Data generated in this study can be found at www.ncbi.nlm.nih.gov/geo/ under accession code GSE194098. All data needed to evaluate the conclusions in the paper are present in the paper and/or the Supplementary Materials.

Submitted 24 May 2021
Accepted 25 January 2022
Published 16 March 2022
10.1126/sciadv.abj6526